POLITECNICO DI TORINO

Master's Degree in Mechatronic Engineering

Master's Degree Thesis

Characterization of the magnetic coupler for a dynamic inductive power transfer system

Supervisors

Prof. Paolo GUGLIELMI

Prof. Marina PERDIGÃO

Candidate

Matteo BULFARO

December 2022

Dedicato a mio zio Pasquale

Acknowledgements

Prima di procedere con la trattazione vorrei ringraziare il mio relatore Paolo Guglielmi e la professoressa Marina Perdigao che mi hanno seguito, insieme allo studente di dottorato Valter Costa, durante i mesi di lavoro a Coimbra e in Italia. Grazie a questa tesi ho avuto modo di approfondire le mie conoscenze tecniche e apprendere nozioni che sicuramente saranno utili per il proseguo della mia carriera.
Mia madre, mio padre, mia sorella e i miei zii Mario e Pasquale mi hanno sempre sostenuto in ogni momento di difficoltà, mi hanno sempre dato grande fiducia anche nelle scelte importanti e perciò sono un esempio e grande motivo di orgoglio, insegnandomi cosa davvero conta nella vita. Grazie ad ogni membro della mia famiglia, dai più vicini ai più lontani, che mi hanno sempre apprezzato e trasmesso nobili valori.
Negli ultimi mesi si sono aggiunti alla mia vita nuovi e importanti amici, ma con i ringraziamenti inizierei da quelli storici, da coloro che ci sono sempre stati fin dalla scuola elementare e sono Gaspare e Smaurito. Loro mi conoscono come pochi e insieme abbiamo condiviso sempre tutto fin dai tempi della bici (secoli fa ormai), abbiamo passato e passeremo momenti bellissimi insieme. Per loro un abbraccio e un augurio di buona fortuna per tutto.
Questo traguardo è anche in parte di Troiano, Ragazzo, Gianluca, Carlo e Claudia con i quali abbiamo condiviso ore e ore di studio insieme, dove i problemi di uno diventavano problemi di tutti come una grande famiglia: quanti esami superati grazie a loro!
Grazie a Giosuè, amico fraterno (quasi twins) al quale voglio molto bene e a Peppe, consigliere per me da anni e che stimo infinitamente.
Grazie ai miei amici Patrizia, Antonio Campanale, Ciro, Alessia, Giovanni, Angelo, Klaris e Riccardo compagni di mille avventure. Sono stati spendidi compagni di viaggio Antonio D, Luca e Vito con i quali voglio condividere questo traguado.
Grazie a tutti gli amici conosciuti in erasmus che hanno visto nascere questo lavoro e con i quali ho passato momenti bellissimi e intensi. Grazie anche alla mia "eredità" di Coimbra: Lorenza, una parola è troppa e due sono poche.
Vorrei infine ringraziare tutte le persone che, anche se non citate, ho incontrato nel mio cammino e che mi hanno regalato anche solo un sorriso o una battuta veloce.

Summary

The market for electric cars is growing more and more. The environmental benefits they bring, particularly in inner city areas, are considerably greater than those of a conventional internal combustion car.

One of the most studied aspects, given the big steps forward that electric technology has made over the years, is the charging of the battery of vehicles and how to optimize it. Several solutions have been presented over time and this document aims to analyze one of these: inductive (wireless) charging. In particular, this technology allows to charge the car both in case of parking and in case of movement, talking respectively of static Inductive power transfer and dynamic Inductive power transfer.

The core of the IPT system is the magnetic coupler: the electromagnetic part that allows to exchange energy between the power supply (primary coil) and the receiver (secondary coil). The purpose of the work is to characterize the behavior of this part of the system in terms of mutual inductance M and coupling factor k in a dynamic situation. Different working conditions were analyzed with multiple geometric configurations between the primary and secondary coil and for each of them the behavior of M and k, combining the graphs together in order to identify the critical aspects in the design of such a system.

The final part encapsulates the mechanical improvement work done on the in-wheel IPT technology prototype pesent in the Laboratório de Sistemas Energéticos (LSE) of Instituto de Telecomunicações (IT) located in the Departamento de Engenharia Eletrotécnica e de Computadores (DEEC) of Universidade de Coimbra (UC) in order to adapt it to a dynamic situation. For it to be used for this purpose, further work is planned which has not been addressed here.

Table of Contents

List of Figures

Acronyms

AC
: Alternating Current

AG
: Air Gap

BEV
: Battery Electric Vehicle

C_i
: Compensation capacitor of i-th primary pad [F]

C_s
: Compensation capacitor of secondary pad [F]

CO2
: Carbon dioxide

DC
: Direct Current

DIPT
: Dynamic Inductive Power Transfer

EMF
: Electromotive force [V]

ESP
: Electronic Stability Control

EV

Electric Vehicle

HEV

Hybrid Electric Vehicle

HF

High Frequency

ICE

Internal Combustion Engine

IPT

Inductive Power Transfer

inWIPT

in-Wheel Inductive Power Transfer

k

Coupling factor

L_i

Self-inductance of i-th primary pad [H]

L_s

Self-inductance of secondary pad [H]

L_{t_i}

Equivalent self-inductance of i-th primary pad in series with secondary one [H]

LD

LateraL Displacement (misalignment) [cm]

M

Mutual inductance [H]

MC

Magnetic Coupler

NC

Nominal (working) conditions

PHEV

Plug-in Hybrid Electric Vehicle

P

Active Power [W]

PD

Primary Distance: distance between primary pads [cm]

R_l

Load resistance [Ω]

R_i

Resistance of i-th primary pad [Ω]

R_s

Resistance of secondary pad [Ω]

rpm

Revolutions per minute [s^{-1}]

S

Apparent power [W]

SIPT

Static Inductive Power Transfer

WPT

Wireless Power Transfer

Chapter 1

INTRODUCTION

The first project of an Electric vehicle (EV) is attributed to the Hungarian priest and physicist Ányos Jedlik who in 1828 invented first prototype of a small car powered by a electric motor that he developed. Few years later Thomas Davenport built a similar contraption which operated on a short, circular, electrified trac: the first prototype of electric locomotive was made [1]. Almost 200 years later the technology of EVs has reached unimaginable levels to the point of having hybrid or totally electric cars at very affordable prices. They are powered by electricity supplied by the battery and propulsion is provided by one or more the electric motors. The main difference between electric and combustion vehicle is the much lower production of CO2. This guarantees an improvement of the quality of the air, a reduction of the noise and consequently an improvement of the life of everyone. Nowadays, the key aspect of the electric mobility is the battery life, the vehicle autonomy and how to charge it. Two big categories of energy transfer are present: with or without wires, wether there is a physical connection between the vehicle and the off-charger or the power transfer is made wirelessly. The second one is an improvement of the wire charging and in last years a lot of research has been done on this topic since no cable is needed, a more convenient recharge is offered and there is the possibility to have a recharge wireless during the motion.

The document starts with an overview on the world of the electrical-mobility and EVs in particular, how the wireless charging works focusing on the inductive power transfer (IPT). The two different kind of IPT are presented: static (SIPT), where the EV is parked, and dynamic (DIPT), where it is in motion. The principle is based on two coils (pads), an AC current is injected in one of them (primary coil) and a voltage is induced in the second one (secondary coil) [2]. These two coils are the magnetic coupler (MC) of the system. The main goal of this work is to characterize the magnetic coupling in terms of mutual inductance (M) and coupling factor (k) during the motion of the EV. Experimental data from the prototype in Laboratório de Sistemas Energéticos (LSE) of Coimbra were used to do this. Some nominal conditions were chosen in order to understand the behaviour of the MC when the working conditions are changed, in this way it is possible to have a clear idea of what aspects to focus on during the design procedure of an DIPT system. Further work was done on the prototype building 3 identical pads. The last part is dedicated to the in-wheel prototype, where a wire support was designed at CAD and printed using a 3D printer.

The work was made in the Laboratório de Sistemas Energéticos (LSE) of Instituto de Telecomunicações (IT) located in the Departamento de Engenharia Eletrotécnica e de Computadores (DEEC) of Universidade de Coimbra (UC) during the Erasmus mobility at Instituto Politécnico de Coimbra under a collaboration protocol between Instituto Superior de Engenharia de Coimbra and Instituto de Telecomunicações. The duration of the mobility has been of 5 months for Master thesis of the Erasmus Mundus Joint Master Degree - Sustainable Transportation and Electrical Power Systems. The work is presented to the committee of program during September 2022. The local supervisors is the professor Marina Perdigão. Aid from all members of LSE was received. The Italian supervisor is the professor Paolo Guglielmi, teacher and researcher at Politecnico di Torino.

Chapter 2

ELECTRICAL MOBILITY

The world of electrical mobility changed rapidly in the last two decades. Every kind of transport was converted in electric: buses, cars, scooters, motorcycles and even the bikes. In Italy during 2021 were circulating twice as many EVs as in 2020 [3].

2.1 Environmental impact of transportation

The global transition to electric mobility is a process that is involving a large part of the industry production. Nowadays the impact on the environment is one of the most important aspects of taking into account by choosing a transport.

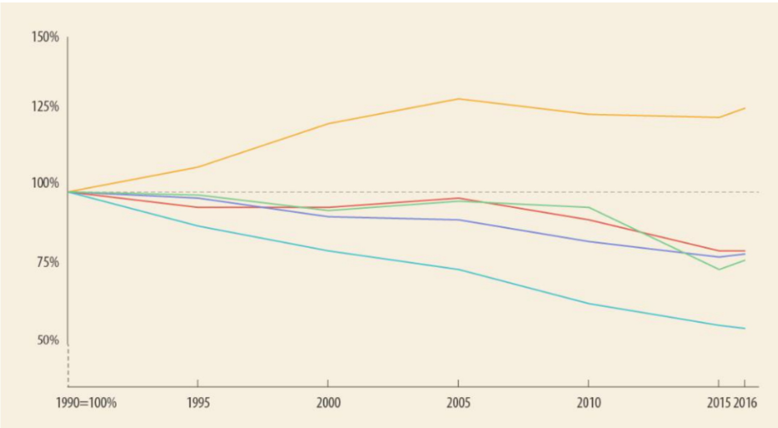

Figure 2.1: CO2 production for different sectors [4]

The curves in figure 2.1 present the CO2 production for different sectors: transport (yellow), agriculture (blue), industrial (sky blue), residential (green) and the energy supply (red). It is evident that the only sector that during the years increases the quantity of CO2 produced is the one related to the transport. This date takes into account only CO2 emissions and no other gases like the NOx but it is an evidence of how the world of transportation, at least until some years ago, was not focus on green mobility.

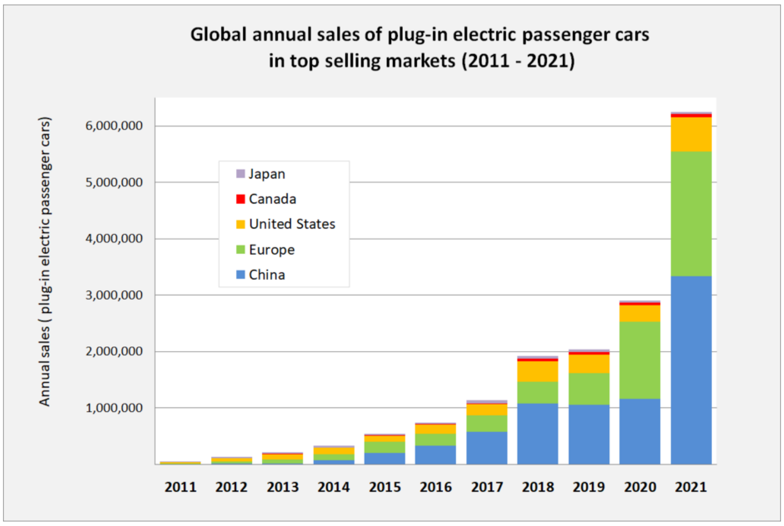

Figure 2.2: Sales of EVs in different Country [5]

Figure 2.2 shows the increase of EV sales, in particular from 2017 onwards. In this way it is possible to decrease the pollution given by transportation. In fact, how the figure 2.3 shows, the environmental impact of the EVs is much less than a combustion vehicle in particular when renewable energies are used. Indeed it is evident that using the renewable energy the impact is much less than the other case because there is the possibility to use green energy.

Exhaust gases are not the only aspects considered for the environmental impact assessment, it is important to take into account the entire life cycle of the vehicles, in particular cars, starting from production and ending with the disposal at the end of life. Important terms concern pollution for the production of batteries and how they can be re-used when exhausted. The variety of existing types of batteries and their different environmental impacts makes it difficult to make comparisons and to arrive at average assessments on the fleet of vehicles in circulation. For electric cars it is however established that batteries, like many other electrical and electronic devices today, are responsible for the greater term of pollution, also because of their criticality compared to other components of the vehicle. With regard to batteries, the first models had significant environmental pollution effects from nickel and cadmium, due to mining, battery manufacture, landfill with possible subsequent oxidation, breakage, infiltration and run-off in the case of no NiCd batteries at centres that route them to specialised units. The problem has been overcome by

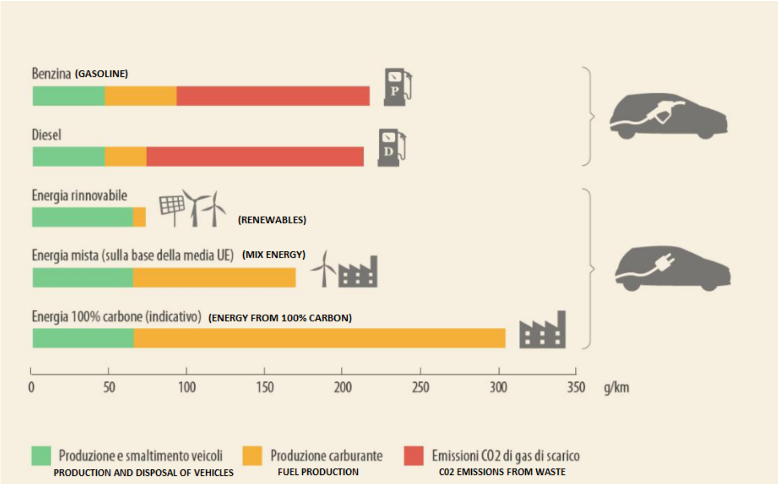

Figure 2.3: Impact of electric and engine vehicles [4]

prohibiting or limiting these compounds in batteries, moreover it is increasingly facilitated the restoration or reuse of automotive batteries for other purposes or the recycling and recovery of materials there. As for their useful life, it is generally guaranteed for 8 years with a real distance estimated in 150 000 km over 10 actual years of use. A potential advantage of electric vehicles compared to traditional ones is driving in congested traffic situations with long stops or very low gait, typical of large cities with high traffic density. In this case the electric means allow to reduce the energy used for transport and do not produce locally pollutants during or for the use of the vehicle. In these situations, an equivalent heat engine medium has very low efficiency and, although waste can be reduced with engine start and stop devices, there is still strong local air pollution, also for reducing the effectiveness of catalytic devices [5]. It is possible to conclude that in terms of production and disposal, electric vehicles are definitely more impactful than combustion vehicles because the battery pack has a strong weight in these terms. On the contrary, in everyday use, electric vehicles, in particular using energy from renewable sources, offer great advantages in terms of the environment and quality of life. An encouraging aspect for EVs is that the research on them is very young, on the contrary for the internal combustion vehicles have been decades that invest resources to improve every aspect, so you expect an ever better future for EVs from every point of view.

2.2 Types of electric vehicles

The EVs are divided into 3 big categories in accordance with the kind of energy source, as depicted in figure 2.4:

- Battery Electric Vehicles, also called BEVs and more frequently called EVs, are fully electric vehicles with rechargeable batteries and no combustion engine. All energy to run the vehicle comes from the battery pack which is recharged from the grid. BEVs are zero emissions vehicles, as they do not generate any harmful tailpipe emissions or air pollution hazards caused by traditional gasoline-powered vehicles [6].
- Hybrid Electric Vehicles, or HEVs, have both a gas-powered engine and an electric motor to drive the car. All energy for the battery is gained through regenerative braking, which recoups otherwise lost energy in braking to assist the gasoline engine during acceleration. In a traditional internal combustion engine vehicle, this braking energy is normally lost as heat in the brake pads and rotors. Regular hybrids cannot plug into the grid to recharge and cannot charge with EVgo [6].
- Plug-in Hybrid Electric Vehicles, or PHEVs, have both an engine and electric motor to drive the car. Like regular hybrids, they can recharge their battery through regenerative braking. They differ from regular hybrids by having a much larger battery pack, and being able to plug into the grid to recharge. While regular hybrids can (at low speed) travel 1-2 miles before the gasoline engine turns on, PHEVs can go anywhere from 10-40 miles before their gas engines provide assistance. Once the all-electric range is depleted, PHEVs act as regular hybrids, and can travel several hundred miles on a tank of gasoline. All PHEVs can charge at an EVgo L2 charger, but most PHEVs are not capable of supporting fast charging [6].

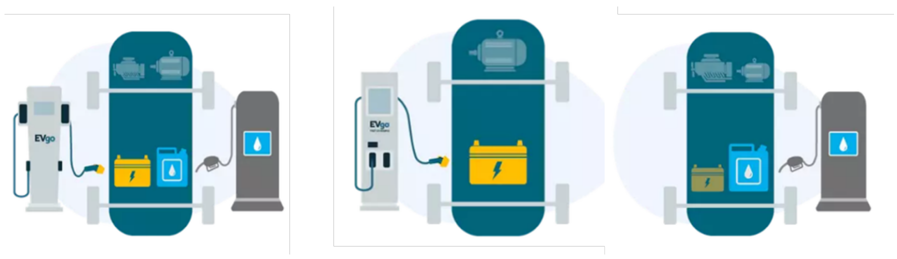

Figure 2.4: BEVs - PHEVs - HEVs [6]

There is a growing demand for non-fossil fuel based and safe electric vehicles. These vehicles bring high investment in fast-charging applications. As per global outlook 2021, despite of pandemic the electric vehicles globally registered is 3 million, 41 % more than for previous year in the more than 60% share belongs to BEVs, as depicted in Fig. 4. This figure presents clear deviation from the progress rates of 2013-2020. At the end of the year 2020 electric vehicles on the road reached more than 10 million. As per survey conducted by IEA (International Energy Agency), the global EV stock (excluding two/three wheelers) expected to reach 145 million at the year 2030 and will have 7 % share of the global vehicle Market. Battery electric vehicle (BEV) is anticipated to become the largest EV market, by propulsion, during the forecast period compared to PHEV. As per the present scenario BEV market crossed more than 60 % in EV market. As per the report, The contactless Charging in EV Market is anticipated to develop at a 46.8 % CAGR during period of 2020 to 2027. It can reach 234 million USD by 2027 [7].

2.3 Charging of Electric Vehicles

The battery is the most important, complex and expensive component in the whole vehicle and one of the most critical aspect of the EVs is the charging of it. The time and the cost of charging depends mostly on the size of the battery and of the capacity of the charging station. It is obvious that the faster the charge is and the more expensive the process is. However also other aspects like the temperature and the losses affect the charging process. During the years the battery life is increased a lot, arriving now until 1000 km of driving autonomy with a single charge in the most expensive vehicles [8]. Normally, batteries have low energy density, which makes them weighty, costly and bulky. In addition slow in charging and provides shorter lifetime. Nowadays lithium ion batteries are mostly used in EVs. Battery capacity restricts the cruise range. Adding batteries will increase the cruise range, which further increase the weight and cost of the vehicle [7].

2.3.1 Conductive charging

There are 3 main types of charging stations available, the first 2 in AC and the last one in DC:

- Domestic: it is possible to charge the car using the domestic electrical system. The maximum power and so the charging time is function of the domestic power that normally is about 3 kW, but could be increased until 6 kW still single phase or 10 kW three phase. It is important to consider that only a 50 - 70 % of the total capacity can be used. To use that there are two possibilities: a classical power plug schuko or a wallbox where it is needed a Type 2 cable.
- Public station at low speed: are the most diffused stations and have a power charging around 22 kW three phase. A Type 2 cable is needed.

- Public station at high speed: the charging power is around 50 kW but there are also certain chargers,as Testa ones for example, that have a power of 150 kW. In this case a cable CCS Combo is needed and is a DC system.

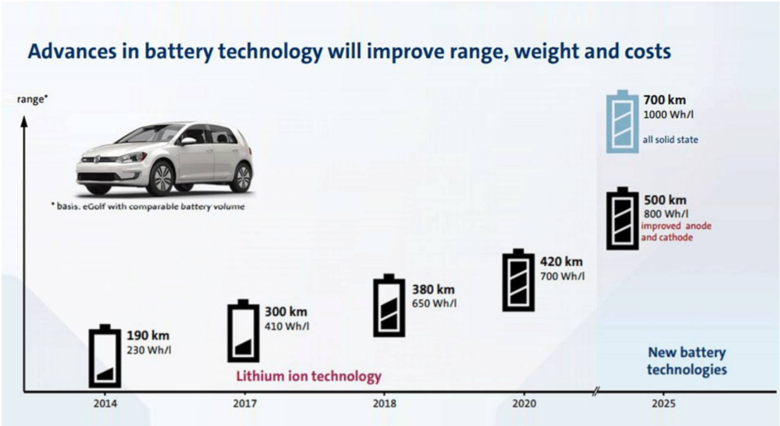

Figure 2.5: Lifetime [9]

Figure 2.6: Schuko, Type2, CCS Combo [9]

In order to have an idea of the time of charging a specific battery it is possible to calculate it by the following easy formula:

$$t[h] = \frac{Capacity\ \ of\ \ battery\ \ [kWh]}{Power\ \ of\ \ station\ \ [kW]} \tag{2.1}$$

For example, taking into account a battery of 45 kWh and a public power station of 22 kW, the car will be fully charged, if totally discharged, in about 2h. It is important to consider aspects like the maximum acceptable power of the battery in order to avoid to damage it. Moreover the losses and heat dissipations affect the charging process. Figure 2.7 presents different sizes of batteries and the time of charging with different capacity of the charging station. It is not comparable with that of combustion vehicles, where a full charge of fuel is made in around 2 or 3 minutes. Therefore the distribution of charging stations where to charge the

Battery capacity	Charging point power 3,7kW	Charging point power 7,4kW	Charging point power 22 kW
20 kWh	5h30	3h00	1h15
30 kWh	8h00	4h30	1h30
40 kWH	11h00	5h45	2h
50 kWh	13h30	7h00	2h30
60 kWh	16h15	8h30	3h00
70 kWh	19h00	10h00	3h30
80 kWh	21h45	11h30	3h45
90 kWh	24h30	1h00	4h30
100 kWh	27h00	2h15	5h00

Figure 2.7: Recharge duration for different station

EV during the period of parking, avoiding queues too long in the charging points, and the speed charging are important constraints on the use of the EVs. Some authors presented fast battery charging methods to minimize the full charging time for less than 30 min. However, available fast charging systems are costly and complex in control. Still, the charging time of the battery is higher than the time to refuel a car based on fossil fuel. Another solution proposed is based on the use of "swapping stations" where the depleted EV batteries are exchanged with fully charged batteries. For the development of EVs, charging systems are playing the main role [7].

2.3.2 Wireless charging

An alternative to wire charge stations is the wireless power transfer (WPT) technology. In order to avoid a physical connection between the charging station and the EV with the time this technology was developed and became a competitive solution comparing to wired charging systems [7]. In a wireless power transmission system a transmitter device, driven by electric power from a power source, generates a time-varying electromagnetic field, which transmits power across space to a receiver device, which extracts power from the field and supplies it to an electrical load [10]. Figure 2.9 presents a block-scheme for a generic WPT system. WPT can be divided in two categories, near-field and far-field:

- In near-field or non-radiative techniques, power is transferred over short distances by magnetic fields using inductive coupling between coils of wire, or by electric fields using capacitive coupling between metal electrodes, however inductive coupling is the mostly used. Its applications include charging handheld devices like phones and electric toothbrushes, RFID tags, induction cooking, and wirelessly charging or continuous wireless power transfer in implantable medical devices like artificial cardiac pacemakers, or electric vehicles [10].

- In far-field or radiative techniques, also called power beaming, power is transferred by beams of electromagnetic radiation, like microwaves[8] or laser beams. These techniques can transfer energy for longer distances but must be aimed at the receiver. Proposed applications for this type include solar power satellites and wireless powered drone aircraft [10].

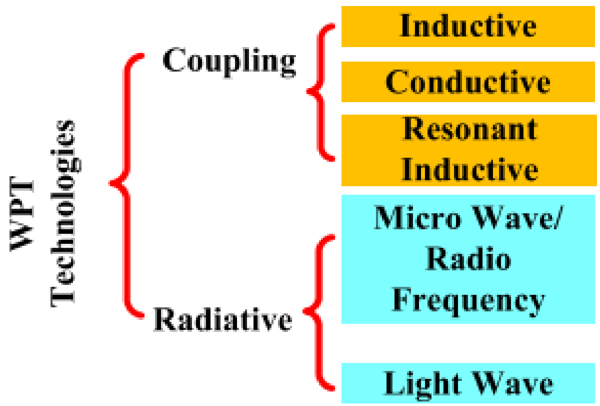

Figure 2.8: WPT topologies [7]

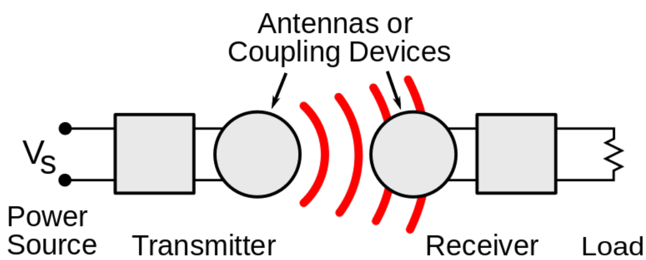

Figure 2.9: WPT generic block [10]

Inductive power transfer (IPT) present some advantages as: no different type of connection are needed (Practicality), no people are needed to plug and unplug (Automation), no wear in the cable and terminals (Durability), no contact for the user with electrical parts (Safety), to have a dynamic charge (Improvements). This advantages makes Wireless technology suitable for large scale implementation.

In the next chapter, the IPT principle of operation is further explained, and the differences between static and dynamic IPT will be presented.

Chapter 3

INDUCTIVE POWER TRANSFER

This chapter introduces wireless power transfer, focusing on the inductive power transfer system (IPT). The formulas that characterize the system starting from the basic physical principles and the different kinds of systems as the static and the dynamic IPT are analyzed. After this a real application of the SIPT to public transport in Turin is shown.

3.1 Electromagnetic notions

The inductive power transfer phenomena is governed by two main formulas: the Ampere's law (3.1), also known as the 4th Maxwell equation, and the Faraday's law (3.2). The first states that the circuiting of the magnetic field B along a closed line is proportional to the size of that electric current I with a constant of proportionality μ equal to the permeability of free space. Faraday's one states that the magnitude of the EMF e induced in a circuit is proportional to the rate of change with time t of the magnetic flux Φ that cuts across the circuit. It can be expressed like (3.3) in case of coil of wire composed by N identical turns.

$$\oint B\,dl = \mu_0 I \tag{3.1}$$

$$e\ [V] = -\frac{d\Phi(\vec{B})}{dt} \tag{3.2}$$

$$e\ [V] = -N\frac{d\Phi(\vec{B})}{dt} \tag{3.3}$$

The notion of flux is expressed in (3.4) as the integral of magnetic field surface can be rewritten as in (3.5), where the dependence from self-inductance L of the circuit is showed. On the other hand, the inductance L can also be expressed as a ratio of the differential change in the flux linkages to the differential change in the current.

$$\Phi = \iint_S \vec{B}\, ds \tag{3.4}$$

$$\Phi = Li \tag{3.5}$$

$$L = N\frac{d\Phi(\vec{B})}{di} \tag{3.6}$$

Combining equation (3.4) with equation)3.7), knowing that $Hl = Ni$ and $B = \mu_0 H$ where l is the length of the coil and A is the cross section yields:

$$L = \frac{N^2 \mu_0 A}{l} \tag{3.7}$$

In this way it is possible to conclude that the self-inductance restricted to the case of a coil is a purely geometric parameter and is dependent on the number of the turns N, the cross section A and the coil length l. Let now consider two coils that are close enough to induce a voltage on each other, similar to what happens in a IPT charging system. A current i_1 time varying in coil-1 estabilishes a magnetic flux Φ_1 that induces a EMF in coil-1 and a part of this flux, called $\Phi_{12} = k_1\Phi_1$, links coil-2 and induces a EMF (e_2) in coil-2. The term k_1 defines the fraction of the flux of coil-1 linking coil-2.

$$e_2 = N_2\frac{d\Phi_{12}}{dt} = N_2\frac{d\Phi_{12}}{di_1}\frac{di_1}{dt} = M_{12}\frac{di_1}{dt} \tag{3.8}$$

where

$$M_{12} = N_2\frac{d\Phi_{12}}{di_1} \tag{3.9}$$

In similar way the current i_2 that flows in coil-2 generates a flux Φ_2 and a part of this flux, called $\Phi_{21} = k_2\Phi_2$, generates a EMF e_1 in coil-1. The term k_2 defines the fraction of the flux of coil-2 linking coil-1, leading to:

$$M_{21} = N_1\frac{d\Phi_{21}}{di_2} \tag{3.10}$$

Then the above expression can be simply written as:

$$M_{21}M_{12} = k_1k_2L_1L_2 \tag{3.11}$$

In a linear system $M_{12} = M_{21} = M$, where M is the mutual inductance of the system with two coils. In this way, replacing $k = \sqrt{k_1 k_2}$ known as coefficient of coupling or coupling factor, equation (3.11) reduces to:

$$M = k\sqrt{L_1 L_2} \tag{3.12}$$

Both k and M are very important in the context of inductive power transfer systems, due to their infuence in the overall energy transfer capabilities. k can have values between 0 (magnetically isolated coils) and 1 (tightly coupled coils) and is a variable that provides a useful measure for directly comparing magnetic properties of different structures. It is the ratio of the flux that links the coils within a pad to the total ux produced by the opposite coil. High values are desired because less magnetomotive force is required to get the same power transfer [11].

3.2 IPT system

In the inductive power tansfer system the power is transferred between coils of wire by a magnetic field. The primary-side or transmitter and the secondary-side or receiver are linked by a transformer through air. This transformer is composed by coils (pads) and they form the magnetic coupler of the system. An alternating current (AC) through the transmitter coil creates an oscillating magnetic field. The magnetic field passes through the receiving coil, where it induces an alternating EMF (voltage), which creates an alternating current in the receiver. The induced alternating current may either drive the load directly, or be rectified to direct current (DC) by a rectifier in the receiver, which drives the load. A few systems, such as electric toothbrush charging stands or mobile phone, work at 50/60 Hz so AC mains current is applied directly to the transmitter coil, but in most systems an electronic oscillator generates a higher frequency AC current which drives the coil, because transmission efficiency improves with frequency [10]. In order to avoid problem of losses and skin effect at high frequency Litz cables are suggested to be used (Appendix A).

The system can be divided in 3 main blocks, as depicted in the figure 3.1: the transmitter (primary) side, the magnetic coupler (MC) and the receiver side. The trasmitter side is composed by an AC-DC converter and a high frequency H-bridge, the magnetic coupler is the link between the two sides and is composed by the coils able to transfer the energy from the primary to the secondary one and the receiver side is located on the EV and is composed by a high frequency AC-DC converter and the battery pack. In both sides a resonant tank is shown which will be presented later. A common design is to use ferrite cores in order to increase the power transfer capability, increasing the MC coupling factor. In SIPT situation it is useful to have the ferrite core in both sids, nonetheless, for DIPT due to the use of multiple transmitter pads and the fragility and cost of ferrite cores, they can be used only on the receiver side.

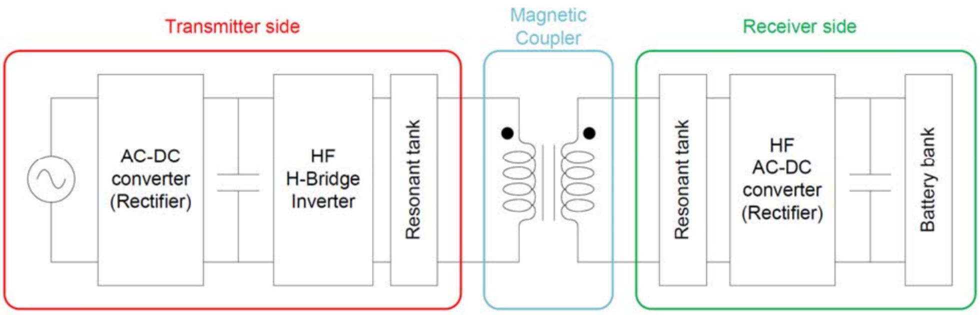

Figure 3.1: IPT detailed scheme

3.2.1 AC-DC converter (Rectifier)

An AC-DC converter or rectifier, converts an AC voltage into a DC voltage. The rule of the full-wave rectifier is to obtain from an AC signal, for example at 50 Hz, a DC one. To do this is important to have an output capacitor, called reservoir capacitor, big enough to have an output signal as constant as possible. In particular the time constant τ (equation 3.13) of the equivalent RC circuit should be much bigger then the input signal frequency in order to have a proper rectification avoiding ripple and noise phenomena.

$$\tau = RC = \frac{1}{2\pi f_c} \tag{3.13}$$

R is the equivalent output resistance seen by the rectifier, C is the reservoir capacitor and f_c is the frequency of the RC system. The high frequency AC-DC converter present in the secondary side of the system is similar to the one described above with the difference that, since the input frequency is high (IPT charging works until 1 MHz), the size of the reservoir capacitor is much smaller than primary one, and fast switching diodes are necessary.

3.2.2 HF H-Bridge inverter

An inverter is a power electronic device that changes direct current (DC) to alternating current (AC) and it does the opposite of rectifiers. In this case the output frequency is higher than the grid frequency, typical values are from 10 kHz to 100 kHz for IPT systems. Since the technology used is the H-Bridge the output wave has a square wave shape.

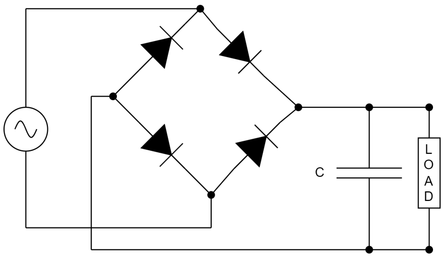

Figure 3.2: Rectifier

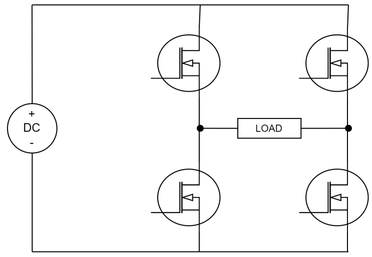

Figure 3.3: H-bridge inverter

3.2.3 Resonant tank

The resonant tank is composed by capacitors and inductors. The goal is to operate at resonance in both the primary and secondary sides of the system in order to reduce switching losses in the H-bridge and avoid hard-switching. Operating at resonance ensures that only the fundamental component of the square voltage wave is responsible for the power transfer for the secondary side (only the active power from the source). The called compensation capacitors are connected, for example, in series or parallel with the MC inductors, in order to compensate the imaginary part of the input impedance to achieve maximum efficiency. Adding a capacitor in series or parallel in the primary and secondary sides allows 4 simple circuit combinations: SS, SP, PS and PP, where the first and second, S or P, stands for primary side and secondary side, Series or Parallel connection between the capacitor and the MC inductor. The capacitors of primary and secondary side are called respectively C_1 and C_s.

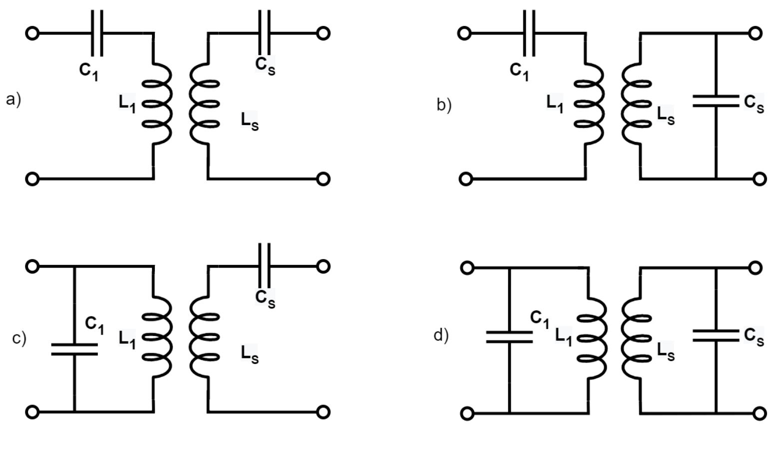

Figure 3.4: SS, SP, PS, PP configurations

3.2.4 Magnetic coupler

The magnetic structure is composed by primary and secondary coils, called also pads. The geometry of the primary and secondary structures, i.e. their coil placement, dimensions as well as the materials used have a great impact on the system performance. In particular, the coupling factor can be improved by proper design of the magnetic couplers. For the DIPT there are two main types of pad:

- Long pad: composed of a single elongated coil, much longer than the pickup size. It has lower construction cost and has a continuous power transfer and a constant coupling factor. The disadvantages are the low coupling factor, the high Joule and iron losses and in case of fault a large part of the road is without power source [2].
- Segmented pad: multiple coils are placed one next to the other, the length of them being comparable to the pickup size. They are easily replacing and have a high coupling factor and mutual inductance having so a better system efficiency. The negative aspects are the necessity to detect approaching and leaving vehicles from segments and the cost, that is higher with respect to the long one. It is also important to optimize the distance between segments using as few pads as possible, thus gaining an economic advantage.

The higher coupling factor and the many fewer losses make the segmtented pads, in the opinion of many studies, better than the elongated one [2]. Focusing on the segmented one, different topologies can be used as Circular Pad (CP), Rectangular pad, double D pad (DDP) and bipolar pads (BPP), as shown in figure 3.5, considering that each topology has advantages and disadvantages.

- Circular pads are widely used for EVs wireless charging system design due to its reduced leakage flux and compact design.
- Double D pads have higher coupling coefficient than circular ones.
- Bipolar power pads are based on DDP topology, but the two coils in the pad are sligthly overlapped, having so better performances in misaligned conditions with respect to the other configurations.
- Double D quadrature pads are based on the DDP topology, and a quadrature coil is added to help boosting the coupling factor with good performances in misaligned conditions. The issue is the size because is bigger than previous one and it increases the cost, in particular for dynamic IPT.

One of the most interesting configurations is the BPP one because has a good coupling profile with horizontal displacement and results similar to DDQP but with an simpler struture due to lower number of coils. The problem of this configuration

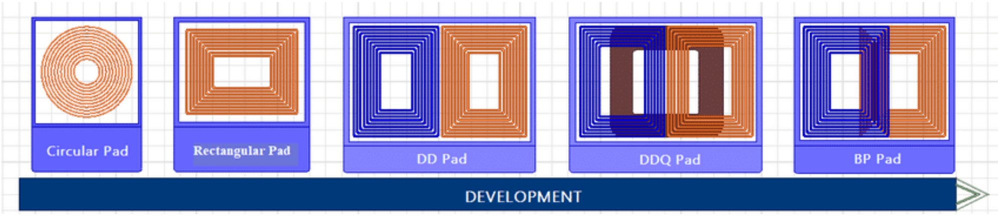

Figure 3.5: Topologies of planar pads

is that, for a dynamic application, the ferrite core present in the primary pads can be easily damaged increasing so the cost of the system. The alternative is to use the same configuration of coils but without the ferrite cores: the behaviour of both is very similar but with lower values of coupling factor and mutual inductance. The advantages of this BPP without ferrite core is that offers a good cost-efficient balance.

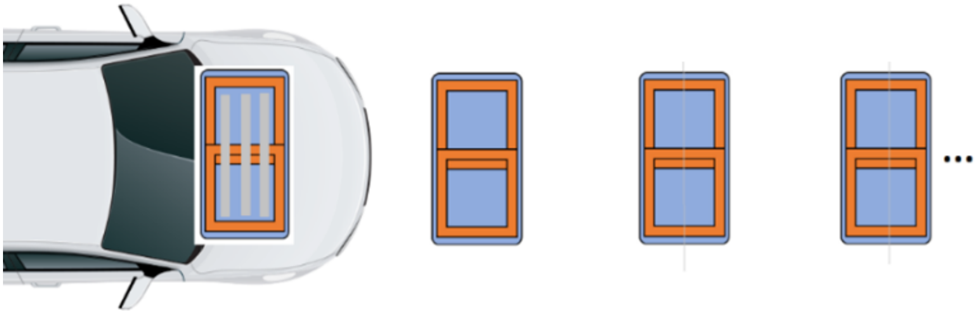

Figure 3.6: Dynamic IPT

3.3 Power transfer capability

In order to quantify the power transfer capability of the structure it is important to take into account the maximum uncompensated apparent power transferred to the receiver path. It corresponds to the product of the open circuit voltage across the receiver and the short circuit current flowing in the receiver:

$$S_{s_u}{}^{max} = V_{s_{oc}} I_{s_{sc}} \tag{3.14}$$

The value of the open circuit voltage (3.15) corresponds to the voltage across the receiver inductance when its terminals are open. On the other hand, the short circuit current (3.16) corresponds to the current in the receiver inductance when its terminals are short-circuited (Figure 3.7) [2] :

$$V_{s_{oc}} = j\omega M I_1 \tag{3.15}$$

$$I_{s_{sc}} = \frac{M}{L_s} I_1 \tag{3.16}$$

$$S_{s_u}{}^{max} = j\omega I_1^2 \frac{M^2}{L_s} \tag{3.17}$$

Where ω is the angular frequency of the power supply, I_1 is the current in the primary circuit, L_s is the self-inductance of the secondary pad and M is the mutual inductance of the magnetic coupler. The term $\frac{M^2}{L_s}$ is called "Power transfer capability" and depends only on geometrical aspects, number of turns and materials. It is much lower than the unit, so the power desired must be achieved working at high frequencies or with high currents. A way to increase the power transferred consists of compensating the system using the principle of resonant tank. In figure 3.7 is reported the case with a series connection of the capacitor [12]. Selecting a

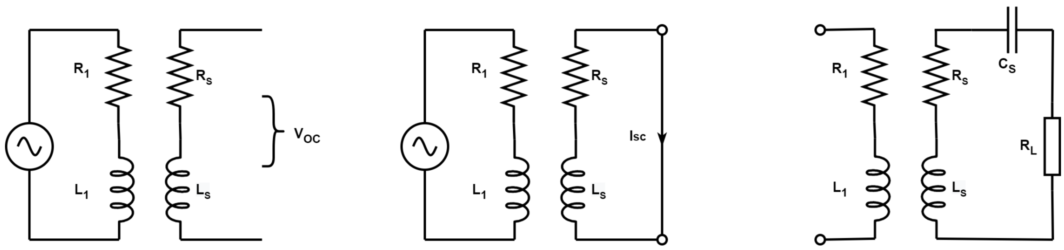

Figure 3.7: Open circuit, short circuit and resonant capacitor scheme

secondary capacitor such as:

$$C_s = \frac{1}{\omega^2 L_s} \tag{3.18}$$

In this way the imaginary part is compensated and the power transferred is increased. At this point the short circuit current is:

$$I_{sc} = \frac{j\omega M I_1}{R_s + j(L_s\omega - \frac{1}{C_s\omega})} = j\frac{M\omega I_1}{R_s} \tag{3.19}$$

The new apparent power of the compensated system is:

$$S_{s_c}{}^{max} = \frac{\omega^2 M^2 I_1^2}{R_s} = S_{s_u} \frac{\omega L_s}{R_s} = S_{s_u} q_s \tag{3.20}$$

It can be seen how the maximum power transferred in a compensated system boosts a factor "qs" respect the uncompensated one. It is the secondary quality factor and that is the relationship between the reactive and active power in the secondary circuit. Considering the real system sourcing a R_L load, the resistance present is no more R_s but $R_L + R_s$. Moreover since the value of the resistance R_s of the pads is very low with respect to the load resistance the term q_s becomes [12]:

$$q_s = \frac{Q_S}{P_s} = \frac{\omega L_s I_s^2}{(R_s + R_L) I_s^2} \approx \frac{\omega L_s}{R_L} \tag{3.21}$$

It would be interesting that this factor was as high as possible, but in case of too high value, the system can lead to being unstable. Typical values of “qs” range between 4 and 10 in most applications. Another way to express the output power is by using the coupling factor “k” [12]:

$$P_{out} = \omega L_1 I_1^2 \frac{M^2}{L_1 L_s} q_s = S_{1_u} k^2 q_s \tag{3.22}$$

$$k = \frac{M}{\sqrt{L_1 L_s}} \tag{3.23}$$

Where k is the Magnetic coupling factor. This coefficient defines the degree of close coupling between the primary and secondary winding. For transferring high power, the value of coupling coefficient must be as high as possible. For SIPT, the coupling coefficient between coils is around 0.1–0.25, if both coils have quality factor around 300 and the efficiency with a theoretical calculation about 96.7%. Efficiency of DIPT also depends on the speed of the EV [13].

3.4 Static inductive power transfer

The IPT is a hot topic in the world of EVs. This technology seems to be able to provide a strong boosting to the development of electric mobility in urban areas. Large scale deployment of Internal Combustion Engine (ICE) based vehicles in transport system lead to the release of harmful fumes into an atmosphere lead to global warming and climate change, which is main concern of global community. Therefore, to lessen dependence on fossil fuel based energy sources and to reduce its harmful impacts on the atmosphere, there is a need for alternative solutions such as EVs charged on renewable energy sources.

Static wireless power transfer refers to the power transfer in stationary condition where both the coupled coils are fixed and aligned to each other. This technique is applicable in many application like charging of mobile phone, biomedical implants and electric vehicles, etc.

In case of vehicles, the IPT setup can be installed at the parking lots or charging stations where EVs stay for long and can get charged. The transmitting coil along with its power supply arrangement are installed under the ground surface and fed by the electrical grid. The power supply can be operated based on the availability or coupling level of a receiver coil. This kind of charging stations are being implemented in many places where the vehicle remains stationary at defined position and IPT coils get coupled. This method provides nice facility at charging station without any manual connections which is safe and hassle free in all weather conditions. The mentioned convenience of wireless charging promotes the use of EVs in market, but static wireless charging also consumes the same charging time of conventional wired chargers.

There are some cars available in the market with the wireless charging setup, for example Chevrolet Volt, Nissan Leaf and Cadillac ELR. There is also a partnership between German vehicle manufacturer Daimler AG and telecommunications chipmaker Qualcomm for developing wireless charging technologies both for in-car applications as well as for recharging electric vehicles without plugging the car into an electrical outlet. Another German vehicle and engine manufacturer BMW AG is developing a wireless inductive charger for its batteries that could be installed in the floor of a garage [14].

Figure 3.8: Inductive electric car charging system at 2011 Tokyo Auto Show [10]

3.4.1 The first bus with inductive charging

The world of wireless electric charging has also taken hold in the world of public transport. In particular, in 2012, the State of Utah had the first electric bus that charges wirelessly. The electric bus is the result of a project carried out by the University of the State of Utah, a major research organization in North America. The vehicle was also the first of its kind to achieve high standards for electric mobility. The electric bus is called Aggie Bus and the wireless charging of an electric bus becomes a smart need: the bus having to make predefined stops, could recharge during its journey. In simpler words, the electric bus stops persso a kind of "pitstop" where a grid will recharge the batteries of the vehicle. The wireless charging technology made a considerable saving on plug-in charging systems, this because the bus driver will not have to manually move any cable so as to avoid any probability of failure. Wireless charging technology eliminates the problem of bulky cables and is strongly weatherproof [15].

Figure 3.9: SIPT example

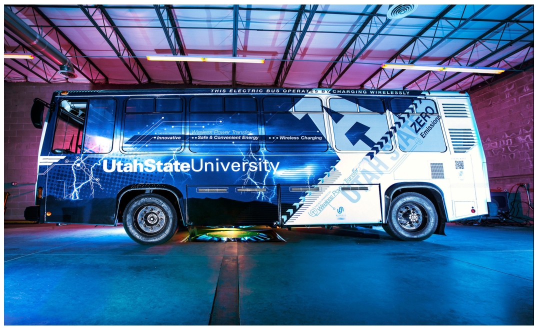

Figure 3.10: Aggie Bus, Utah

3.4.2 Wireless bus charge in Turin

To improve air quality in the historical city centre, Torino decided to convert it into a Limited Traffic Zone (LTZ), allowing access to a limited number of authorised vehicles. Torino launched in 2003 the STAR 1 line. A few months later, on citizens' request, the service was expanded. The line serves essential points in the city centre. Its success led Torino's public transport operator, GTT, to launch STAR 2 in September 2007 to cover crucial areas of the historical city centre, the Porta Susa railway station and to connect with other public transport lines and the metro. Both tracks – each around 13km long – use the inductive charging system.

Electric buses are regarded as more comfortable than their traditional counterpart and produce no local emissions. However, the limited battery and the lack of a network of battery charging facilities have limited their expansion. Inductive charging systems tackle these problems by providing wireless charging points along bus routes. Turin has been using this technology on two of its bus lines for over 16 years.

Each track has a length of approximately 7 km, and the buses are recharged at the terminal stops with an inductive fast charging process. It takes only 7 minutes to recharge to a capacity of 80% (at the depot at the end of the day charging adds the remaining 20%, achieving 200V battery voltage).Wireless opportunity charging helped to significantly reduce the battery capacity required. Instead of driving around tons of batteries, the buses focus on transporting people.

Some data: Two charging points were installed at the end of Turin's STAR 1 line; 10-12 minutes of recharging are enough to keep buses in operation from 07:00 to 20:00. The buses are 7.5 metres long, and their maximum weight is 11,500 kg.

They travel about 130 km a day, accommodate 40 passengers, and their maximum speed is 70 km/h. The 180Ah battery installed on the buses is fed at 336V and produces a power of 65kW. Operating time is 13 hours per day.

Figure 3.11: Turin inductive buses

Chapter 4

DIPT PROTOTYPE

The goal of the chapter is to present the prototype in Laboratório de Sistemas Energéticos (LSE) of Instituto de Telecomunicações (IT) located in the Departamento de Engenharia Eletrotécnica e de Computadores (DEEC) of Universidade de Coimbra (UC). Crucial aspects such as variables that have been modified, pad construction and how to practically measure self-inductance are here presented.

4.1 The prototype

It has a structure in wood with 3 primary pads and an electric motor linked to a screw that has the role to transform the rotational motion of the motor in linear one, moving so the receiver pad to emulates the EV movement. In figure 4.1: 1

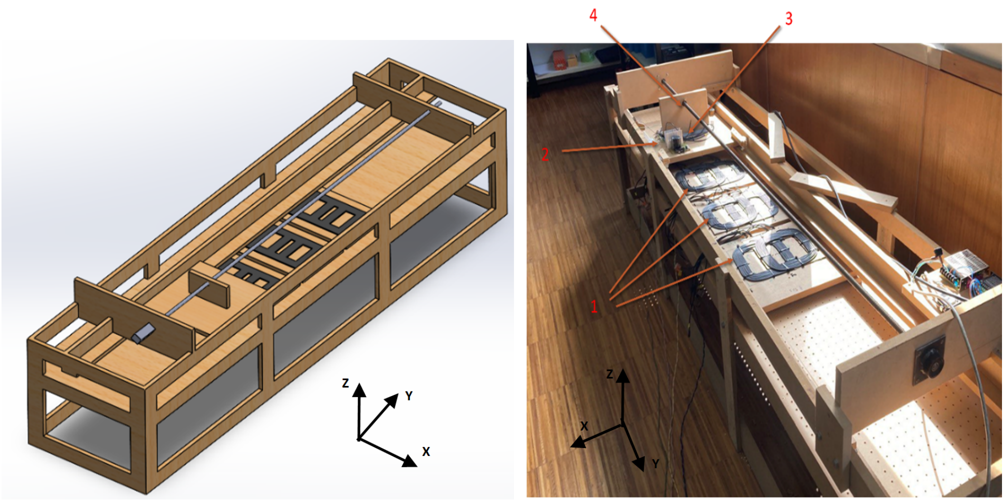

Figure 4.1: DIPT prototype

are the primary pads, 2 is the cart that emulates the movement of the EV, 3 is the ferrite core linked to the secondary pad that is under the cart(not visible in the picture), 4 indicates the threaded to convert the rotary motion of the electric controlled motor in linear movement.

The key parameters (variables) that are considered in order to characterize the dynamic behaviour between primary and secondary pads are:

- Air-gap (AG): Vertical clearance or EV distance to the road, z axis. By changing the distance on the z axis the scope is to understand how the coupling changes with vehicles that have different height, or variations in the vehicle height as it moves, due to bumps or holes in the roadway.
- Primary-distance (PD). In order to avoid to put too much pads on the road would be useful investigate how the coupling changes by changing the distance between primary pads. Distance between primary pads is the y axis distance between them.
- Lateral-displacement (LD). By moving the primary pads on the x-axis the objective is to investigate the behaviour in case of misalignment. Lateral misalignment x axis.

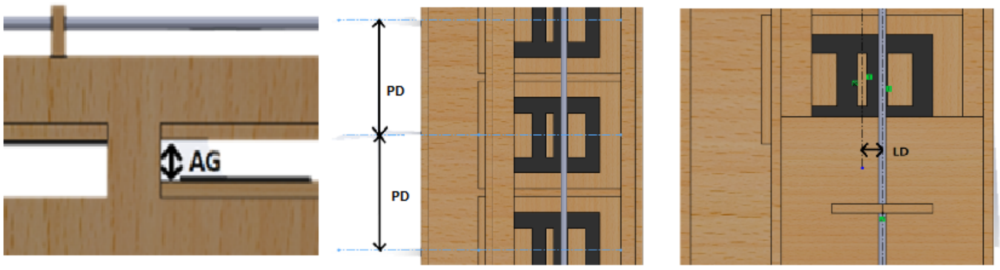

Figure 4.2: AG - PD - LD scheme

4.2 Pads construction

The construction of the pads is a crucial aspect of the prototype since they are the link between the energized side and the side to energize. It is important to take into account the dimension of the pads in order to put in relation it with the different modifiable parameters and so trying to generalize the obtained results. For this work, where the goal is to characterize the behaviour of the MC and not to have the maximum coupling factor possible, to have a easier and cheaper prototype the segmented BPP pads were chosen for both the transmitter and receiver. In particular on the receiver was used the configuration with the ferrite core, instead on the primary pads was not used any of them. Figure 4.3 presents the size, in mm, for the pads. Morover in figure 4.4 the scheme of the secondary pad where a pair of ferrite cores with dimension 28x186 mm is presented. The focus during the

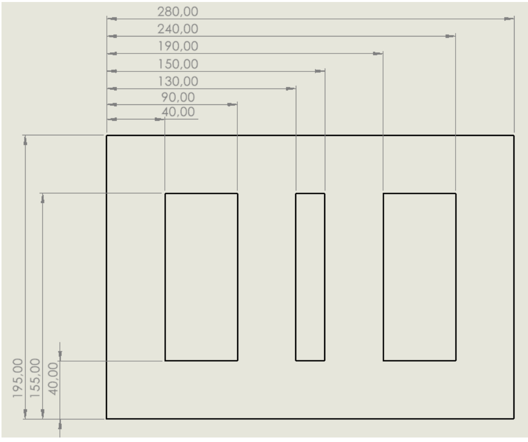

Figure 4.3: Pad dimension

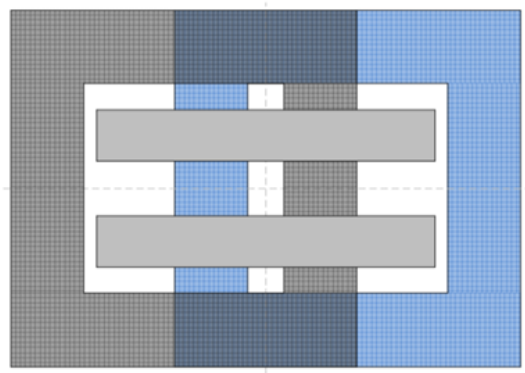

Figure 4.4: Pad scheme with ferrite core

construction of the pads is the value of the self-inductance that is measured with an LCR-meter. In fact, to have reliable values, is important that all the pads have a similar value of self-inductance. This value is strongly affected by the dimension of the pads, the quality of the cable and the number of turns. The goal is to obtain peaks of the curves as close as possible to the same value.

4.3 MC practical calculations

The objective of the work is to characterize the magnetic coupler in terms of self-inductance, mutual inductance and coupling factor, in particular it is interesting to know the coupling factor and the mutual inductance changing the relative position of the secondary pads with respect to the primary ones like shown in figure 4.5. In this section it is described how to do it practically: instrumentation to use, how to set it and how mathematically obtain M and k.

The measurements are taken by using a LCR-meter (figure 4.6) at 10 kHz, properly calibrated. Using this instrument it is possible to calculate, in addition to the resistance, the inductance of the system connected.

In order to calculate the mutual inductance M formulas of series (figure 4.7) and anti-series (figure 4.8) connection between inductance are used:

$$L_{t_+} = L_1 + L_2 + 2M_+ \tag{4.1}$$

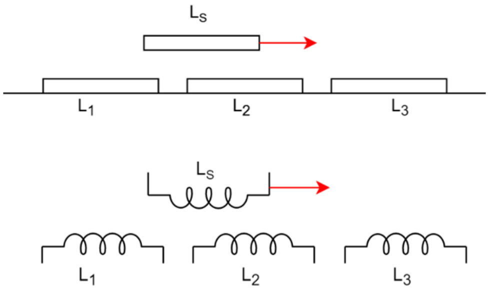

Figure 4.5: DIPT inductances scheme

Figure 4.6: LCR-meter

$$L_{t_-} = L_1 + L_2 - 2M_+ \tag{4.2}$$

Where L_{t_+} and L_{t_-} indicate the total equivalent of the series and anti-series of two coils. Each coil, that in this case is the pad, is affected by the magnetic field generated by the other ones and so the equivalent self-inductance of the series is not only the sum of each self-inductance but it is necessary also to take into account the value of M that theoretically should be the same both series and anti-series. Inverting (4.1) and (4.2):

$$M_+ = \frac{L_t - L_1 - L_2}{2} \tag{4.3}$$

$$M_- = \frac{-L_t + L_1 + L_2}{2} \tag{4.4}$$

It is possible to measure L_t by connecting in series 2 pads (4 coils, 2 for each pad) and to measure the self-inductance of each one, in this way the only unknown member is M. Remembering formula (3.12) it is possible to calculate easily the coupling factor. This situation considers just a couple of coils but the prototype has 3 pairs of coils since the secondary one couples with each one of the 3 primary so it is important to generalize the previous formulas considering that "i" indicates the i-th primary pad and so it varies from 1 to 3. Instead "s" is the acronym to indicate the secondary one.

$$M_{is_+} = \frac{L_{t_i} - L_i - L_s}{2} \tag{4.5}$$

$$M_{is_-} = \frac{-L_{t_i} + L_i + L_s}{2} \tag{4.6}$$

In order to apply these formulas to the dynamical IPT the measurements are repeated, during the front motion of the cart, each 5 cm in order to have a good density of points and build so a good dynamical model. In order to obtain all the

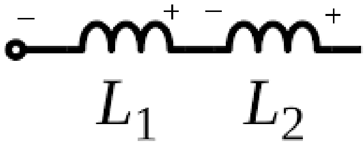

Figure 4.7: Series coils connection

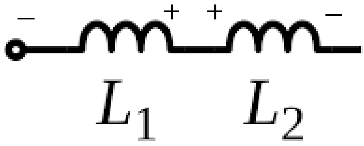

Figure 4.8: Anti-series coils connection

needed values ($L_i, L_s, L_{t_{is+}}$ and $L_{t_{is+}}$), since each pad (pair of coils) has a positive and a negative wires that indicate, by convention, a way of current flowing and so a direction for the magnetic field, the connections shown in figures 4.9, 4.10, 4.11, 4.12 between pads and LCR-meter were made.

If for L_i and L_s the connection between LCR-meter and the pad is easier, explanations are needed for the other two cases:

- $L_{t_{is+}}$ is measured, figure 4.11, by connecting in series, so the "+" of one with the "-" of the other, the L_i under analysis and L_s.
- $L_{t_{is-}}$ is measured, figure 4.12, by connecting in anti-series, so the "-" of one with the "-" of the other, the L_i under analysis and L_s, having so both the positive side of the two pads connected to the LCR-meter

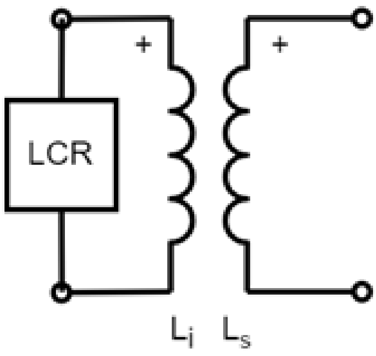

Figure 4.9: L_i measurement

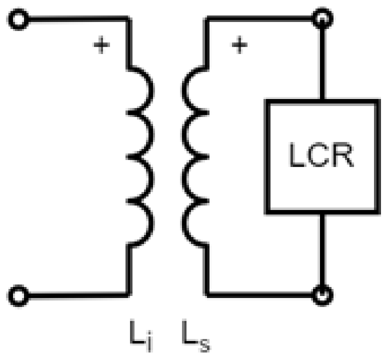

Figure 4.10: L_s measurement

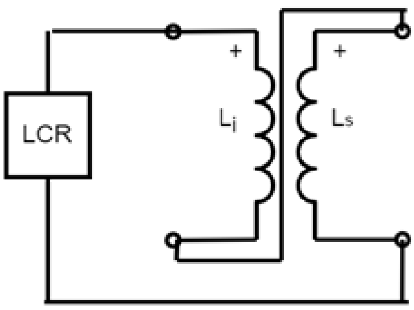

Figure 4.11: $L_{t_{is+}}$ measurement

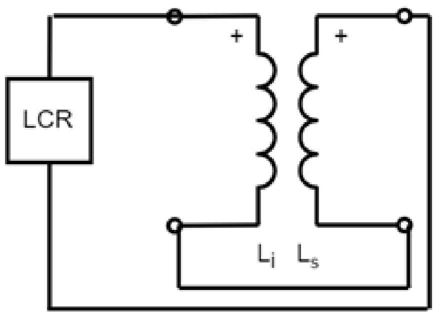

Figure 4.12: $L_{t_{is-}}$ measurement

Chapter 5

MAGNETIC COUPLING CHARACTERIZATION

The goal of this chapter, by using the tools explained so far, is to obtain the graphs of the dynamical behaviour of the mutual inductance and the coupling factor, characterizing so the the magnetic coupling system. In particular it is possible to investigate if, changing the working conditions, there are qualitative and quantitative changes in M and k. The parameters to change in order to fully characterise the system are that presented in 4.1: air-gap (AG), lateral misalignment (LD) and distance between primary pads (PD).

5.1 Tested working conditions

To investigate the effect of the different working situations is possible to taking into account a nominal working condition (NC) in order to obtain a behaviour to compare with the other ones. Below the list of the different working conditions that were tested:

- Air gap 4 cm, 0 cm lateral displacement, 28 cm primary distance (NC)
- Air gap 4 cm, 0 cm lateral displacement, 30 cm primary distance
- Air gap 4 cm, 0 cm lateral displacement, 32.5 cm primary distance
- Air gap 4 cm, 0 cm lateral displacement, 35 cm primary distance
- Air gap 4 cm, 5 cm lateral displacement, 30 cm primary distance
- Air gap 4 cm, 10 cm lateral displacement, 30 cm primary distance
- Air gap 4 cm, 15 cm lateral displacement, 30 cm primary distance

- Air gap 4 cm, 5 cm lateral displacement, 35 cm primary distance
- Air gap 4 cm, 10 cm lateral displacement, 35 cm primary distance
- Air gap 4 cm, 15 cm lateral displacement, 35 cm primary distance
- Air gap 6 cm, 0 cm lateral displacement, 30 cm primary distance
- Air gap 6 cm, 0 cm lateral displacement, 32.5 cm primary distance
- Air gap 6 cm, 0 cm lateral displacement, 35 cm primary distance
- Air gap 6 cm, 5 cm lateral displacement, 30 cm primary distance
- Air gap 6 cm, 10 cm lateral displacement, 30 cm primary distance
- Air gap 6 cm, 15 cm lateral displacement, 30 cm primary distance
- Air gap 6 cm, 5 cm lateral displacement, 35 cm primary distance
- Air gap 6 cm, 10 cm lateral displacement, 35 cm primary distance
- Air gap 6 cm, 15 cm lateral displacement, 35 cm primary distance
- Air gap 8 cm, 0 cm lateral displacement, 30 cm primary distance
- Air gap 8 cm, 0 cm lateral displacement, 32.5 cm primary distance
- Air gap 8 cm, 0 cm lateral displacement, 35 cm primary distance
- Air gap 10 cm, 0 cm lateral displacement, 30 cm primary distance

5.2 Nominal case

In order to better understand the effect of changing the working variables nominal case is considered with: air gap of 4 cm, 30 cm of distance between primary pads and absence of lateral misalignment between primary and secondary pads.

The self inductances L_1, L_2, L_3, L_s are mostly constant (figure 5.1 and 5.2). The peaks of the primary pads are given by the presence of ferrite core in the secondary one and this is the reason for which the self-inductance of the secondary is bigger than the other and constant. The peak of primary ones is in correspondence of the central point of the pad. The mutual inductance has a peak value of about 16.8 μH (figure 5.3) and the coupling factor is 0.33 (figure 5.4). Is important, considering the 3 curves together, notice that the lower value is not so close to zero, about 2.5 μH, so it is sure that energy is always transferred to the secondary pad.

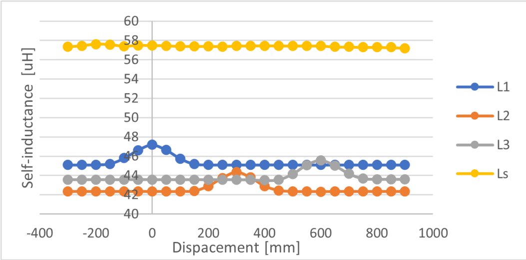

Figure 5.1: Self-inductance

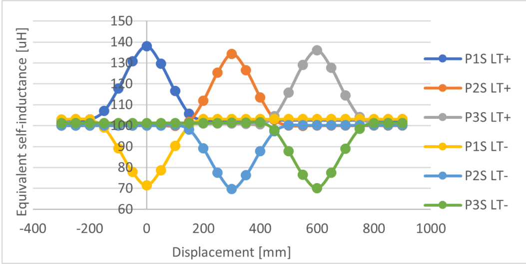

Figure 5.2: L_{t_i}

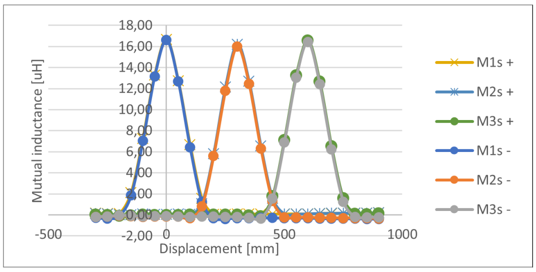

Figure 5.3: M_{is}

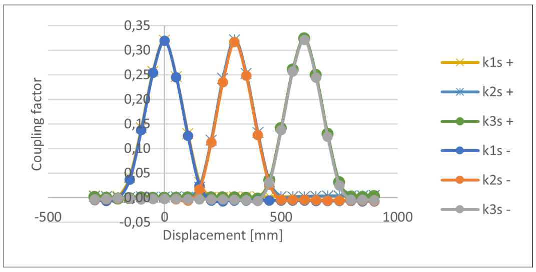

Figure 5.4: k_{is}

5.3 Air-gap variation

The objective is to plot what happens changing the air-gap with constant LD and PD. Different PD values are taken in different graphs: 30 cm, 32.5 cm, 35 cm. Instead LD is always 0 cm. The air gap is an important parameter because takes into account the different height of the EVs.

The most significant change is in the peak value. Considering that the three peaks are more or less constant, it is interesting to calculate the relative percentage change, using the average value, like in 5.1:

$$\epsilon[\%] = \frac{p_{\mathrm{r}} - p_{\mathrm{c}}}{p_{\mathrm{r}}} \cdot 100 \tag{5.1}$$

Where $\mathrm{p_r}$ is the value of the peak of reference with respect to which calculate the misalignment and $\mathrm{p_c}$ is the peak to compare.

Changing of 2 cm the air gap the variation of the peak value is about 35 – 40 %, 55 - 60 % if it is of 4 cm and more than 70 % if it is of 6 cm. It is evident, from figure 5.11, the behaviour is not linear, in particular the peak value decreases less when the air gap is bigger. This is observable with all the different values of primary distance analyzed. Instead the lower value is not affected how the peak one but in general it decrease of few percentuage points by changing the air gap. These conclusions put in evidence how the air gap variable is very important. Indeed the

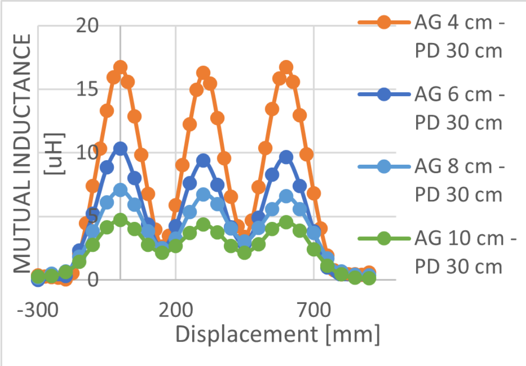

Figure 5.5: M behaviour, different AG, PD 30cm

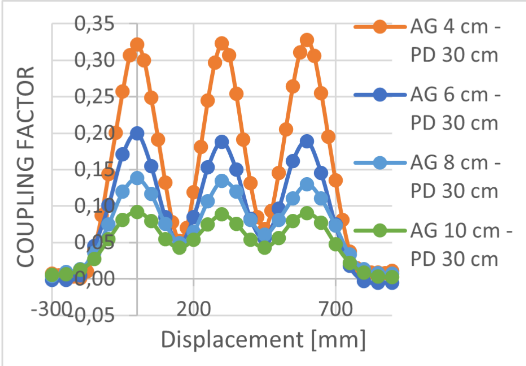

Figure 5.6: k behaviour, different AG, PD 30 cm

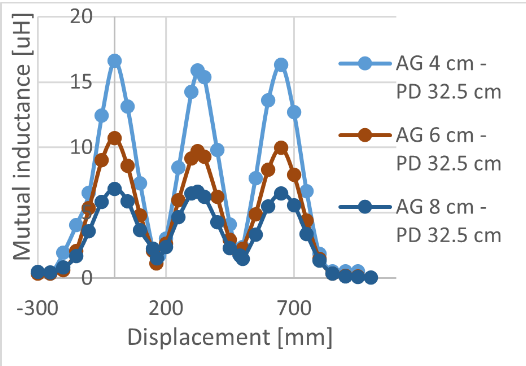

Figure 5.7: M behaviour, different AG, PD 32.5cm

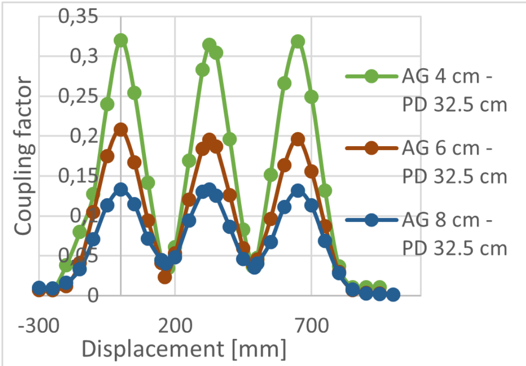

Figure 5.8: k behaviour, different AG, PD 32.5cm

energy that the system gives to the secondary pad is function of the area under the curve and it's evident that a simply change of 2 cm in air gap changes a lot the area. The previous consideration, made for the mutual inductance, are valid also for the coupling factor since it is calculated starting from it.

5.4 Primary-distance variation

The objective is to analyse what happen changing the PD with constant LD and AG. Different AG values are taken in different graphs: 4 cm, 6 cm, 8 cm. Instead LD is always 0 cm. In this way the distribution of the pads on the road is optimized, having so economic advantages.

The most affected parameter is the lower value, instead the peak is mostly constant. Taking into account the average of the lower values with respect to the

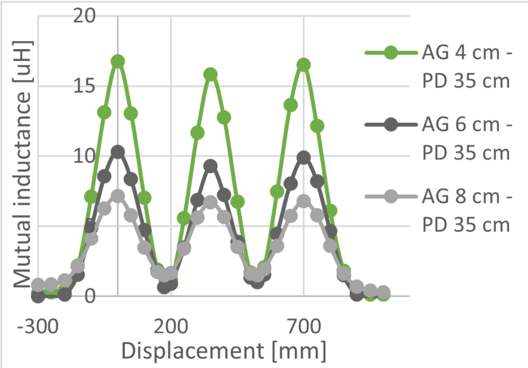

Figure 5.9: M behaviour, different AG, PD 35cm

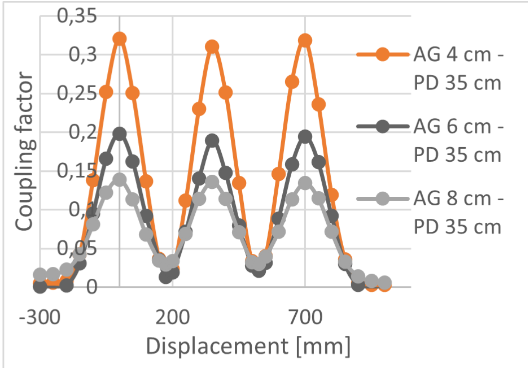

Figure 5.10: k behaviour, different AG, PD 35cm

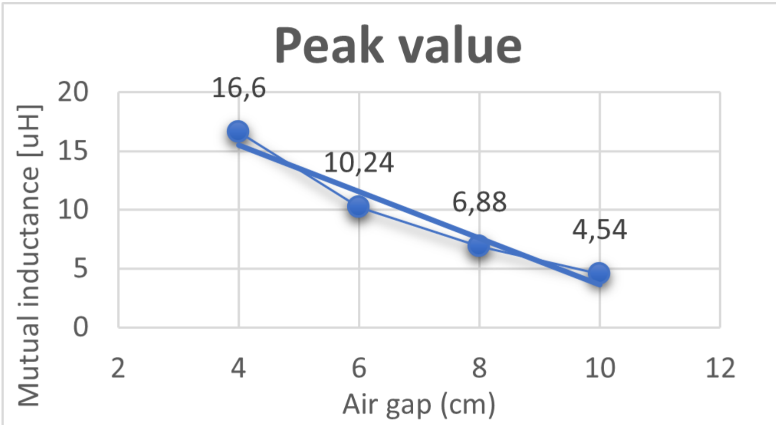

Figure 5.11: Peak values with different AG

primary distance the behaviour 5.20.

Is important to not have a lower value too much close to zero in order to transfer always energy. Air-gap of 8 cm and primary distance of 35 cm (with 0 cm lateral misalignment) is the worst analysed case and has still a lower value of 0.67, this means that there is still margin to increase a bit the primary distance without loss too much in the amount of transferred energy.

5.5 Lateral-misalignment variation

The objective is to analyse what happens changing the LD with constant PD and AG. In order to have a complete view of the behaviour different air gap values (4 cm and 6 cm) and primary distance (30 cm and 35 cm) are taken into account. In this way a realistic situation where the EV is not exactly aligned with the primary

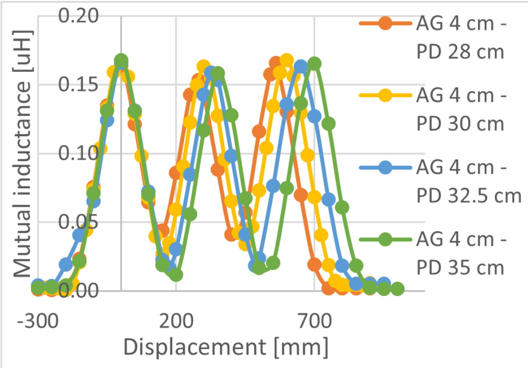

Figure 5.12: M behaviour, different PD, AG 4cm

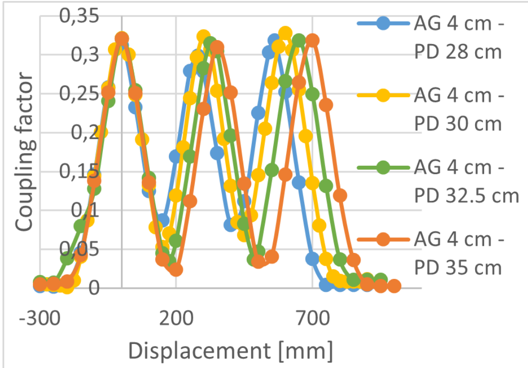

Figure 5.13: k behaviour, different PD, AG 4cm

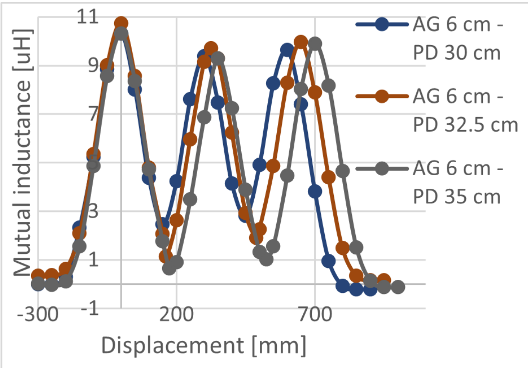

Figure 5.14: M behaviour, different PD, AG 6cm

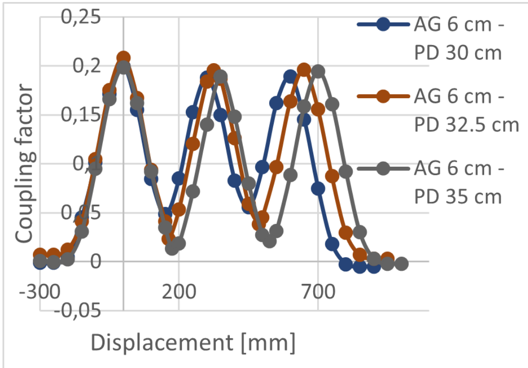

Figure 5.15: k behaviour, different PD, AG 6cm

pads is considered. The comparisons are always made by reference to nominal value and the lateral misalignment analysed are: 0 cm, 5 cm, 10 cm, 15 cm.

The behaviour is the same for all the considered cases. Taking into account the figure 5.19, where in green there is the surface that shows the changes of LD to the nominal case, the values of mutual inductance are getting smaller. In particular, as showed in figure 5.22, the value of mutual inductance decreases until negative values. This is in accordance with the already present case in literature [2]. The critical point, to avoid absolutely in practical situation, is when it is equal to zero because no energy is transferred between pads. Instead when the value is negative it is sure to have coupling between systems.It is negative because of the relative position of the pads and the inverting of the induced flux, due to the direction of the current that produces the majority of the flux at which the receiver is subjected. Thus, the current is in the opposite direction comparing with the position of perfect alignement between pads, which means opposite signal in the flux, which leads to

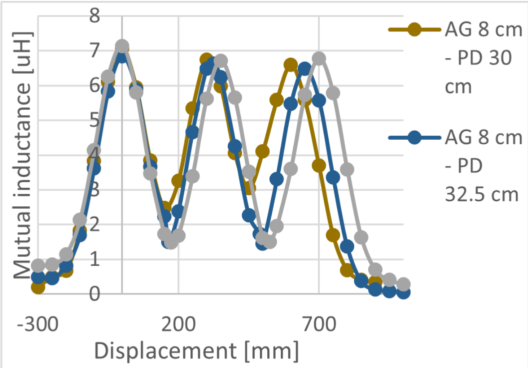

Figure 5.16: M behaviour, different PD, AG 8cm

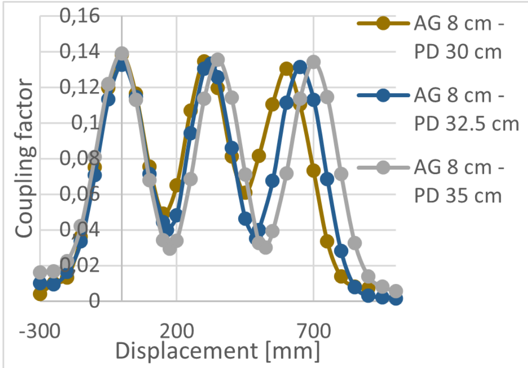

Figure 5.17: k behaviour, different PD, AG 8cm

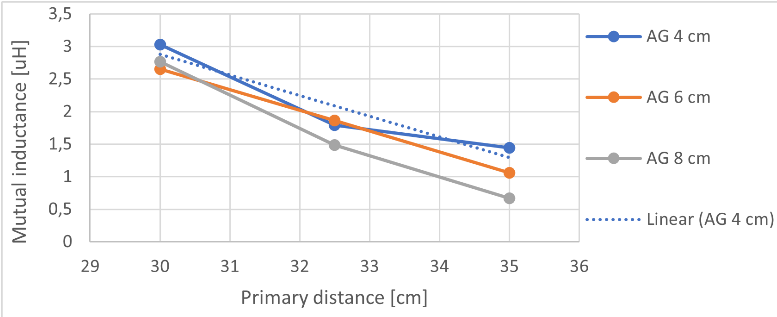

Figure 5.18: Lower values analysis

negative values on the M and k. For these reasons the lateral displacement is an important parameter to take into account in the design of a DIPT network.

What was written for the mutual inductance is replicable for the coupling factor since they are directly proportional (Appendix B for the detailed graphs).

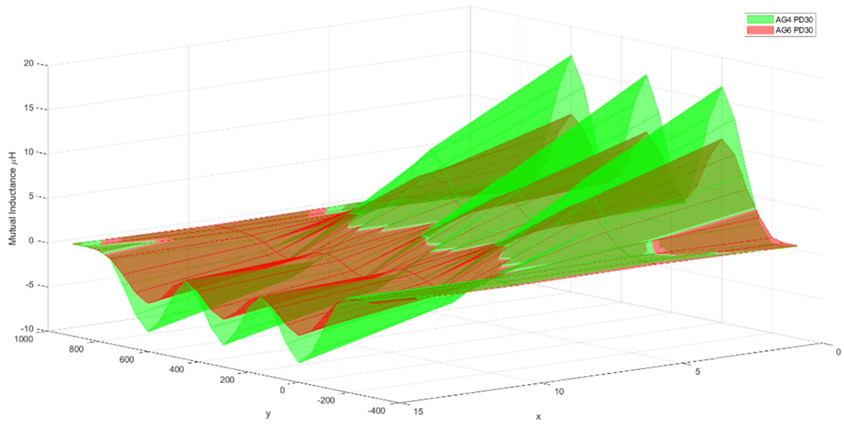

Figure 5.19: Different air gaps with 30 cm primary distance

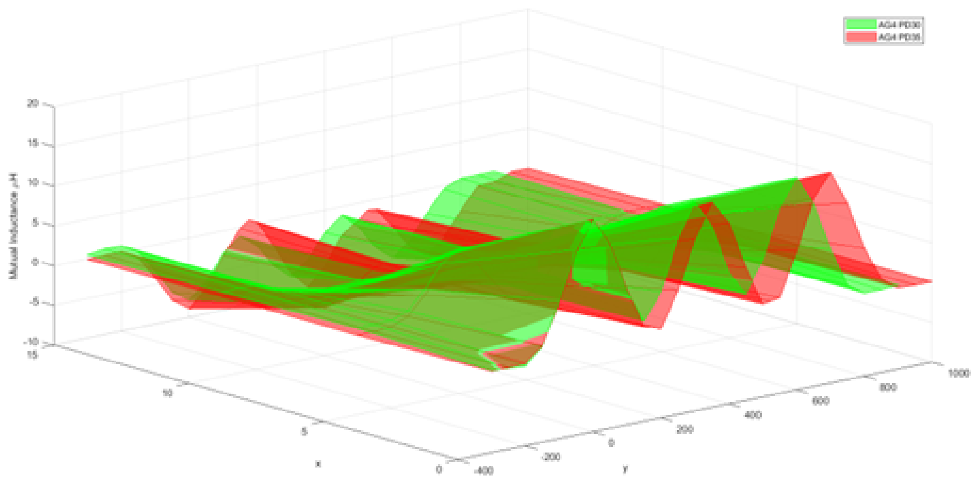

Figure 5.20: 4 cm air gap with different primary distances

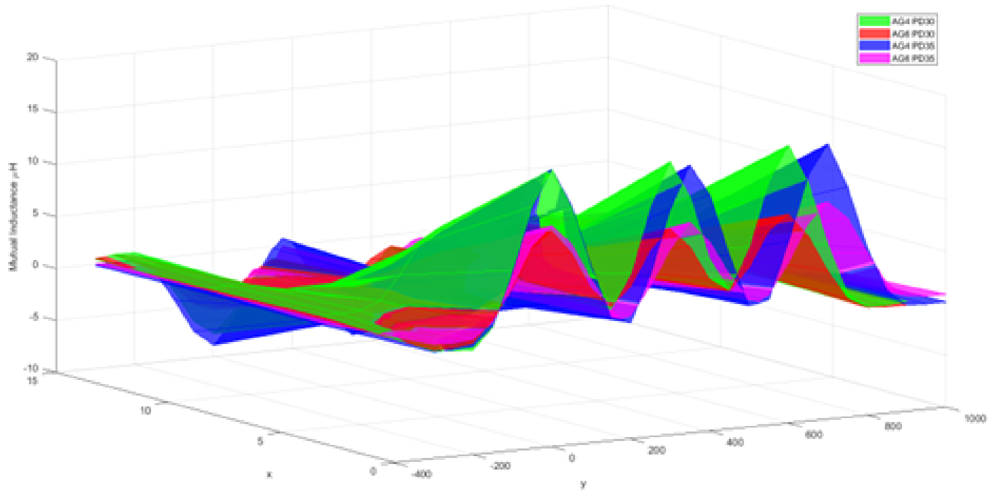

Figure 5.21: M, complete graph

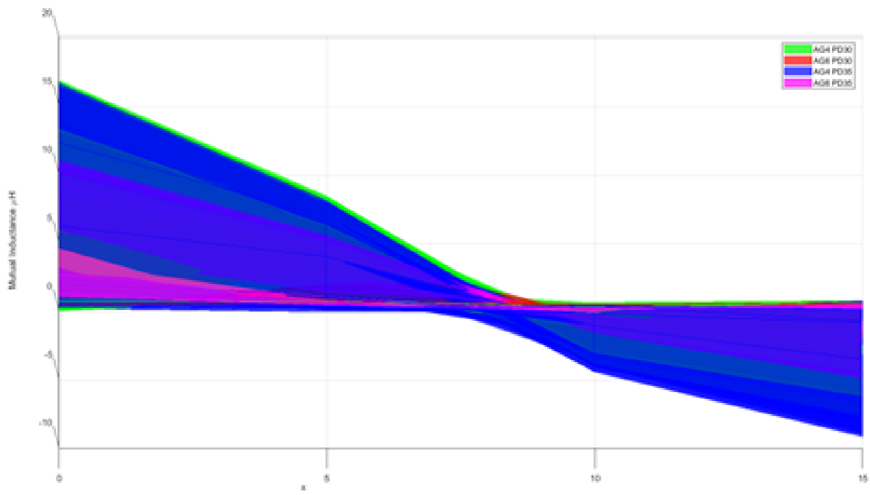

Figure 5.22: Lateral displacement characterization

Chapter 6

IN-WHEEL PROTOTYPE

From previous analysis it is evident that air-gap in IPT has a great impact regardinghas a great impact regarding power transfer capability. In this chapter static in-wheel inductive power transfer (inWIPT) is presented which significantly reduces the issues associated with large air-gaps. The prototype in the Laboratório de Sistemas Energéticos (LSE) of Instituto de Telecomunicações (IT) located in DEEC of Universidade de Coimbra (UC) is explained, focusing on possible future mechanical improvements.

6.1 The technology

The electronic system is the same as that presented in section 3.2 and 3.3 with a substantial difference: the receiver coils, including the hardware units, are inside the tyre (figure 6.1). In this way the tyre is always in contact with the road surface, there is a major reduction in the air-gap an increase in coupling coefficient and mutual inductance. The maximum power transfer depends on several factors such as tyre size, possible wire cross section of the receiving as well as transmitting coil, the possible voltage levels as well as frequency. The receiving coils are mounted on the rim surface inside the tyre due to manufacturing limitations.

6.2 In-wheel prototype

This section describes the initial prototype (figure 6.2) and the modifications that have been made. The initial prototype has a prefabricated wooden structure, including the wheel, with two side supports that have the task of keeping the wheel raised. Two shafts connect these supports with the wheel by means of two SKF bearings. The wheel, the heart of the prototype, has on the outer surface the coils that are part of the MC of the system. The primary pad, in this case only one

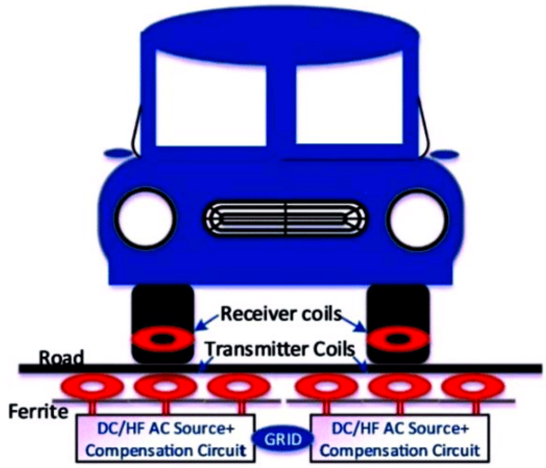

Figure 6.1: In-wheel charging scheme

because it has been thought for a static analysis, is placed under the wheel (figure 6.3) and is free to be moved manually in order to simulate any working conditions different from the nominal ones. The wire that constitutes the secondary pad is fixed to the wheel by means of wooden supports built specifically for the prototype, clearly visible in the figure 6.3.

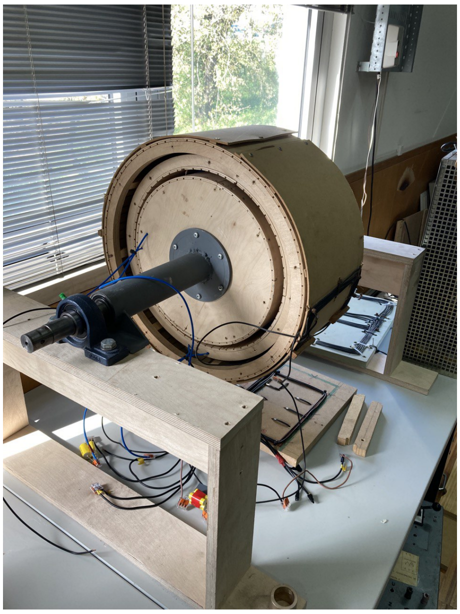

Figure 6.2: Initial prototype

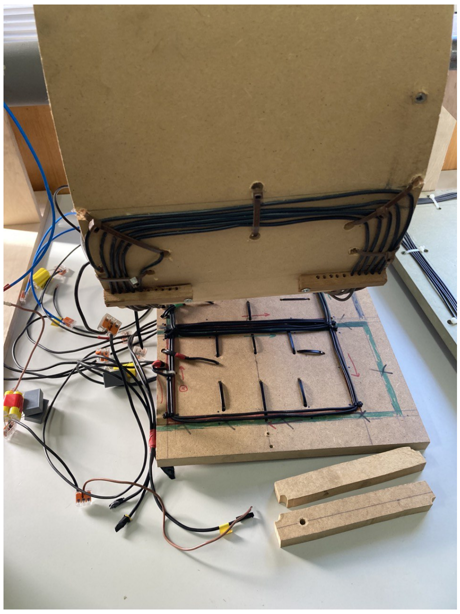

Figure 6.3: Coils zoom

The prototype, in these conditions, is not suitable for any dynamic analysis because no motor able to rotate the wheel is connected, not necessary for the static testing for which it was initially thought, where it is possible just place it and hold it manually. The purpose is to connect an electric motor to the shaft and to create new supports for the wire because the problem of those present is that they do not require a simple removal of the wire.

6.2.1 Motor connection

The connection with an electric motor was indispensable to adapt the prototype to a dynamic analysis. To do this the three-phase electric motor EFACEC UNIVERSAL MOTORS already present in the laboratory was used. The peculiarity is that this motor was already connected to an AC-driver (Yaskawa V1000) capable of adjusting the rotation frequency of the motor shaft. The motor has weight of 9 kg an is a three-phase two-pole asynchronous motor, which with a power frequency of 50 Hz reaches 1375 rpm with a power factor $\varphi = 0.81$. The AC-drive offers the possibility to adjust the input frequency of the motor with a precision of 0.1. It is important to take into account, for motor electric construction, the motor poles, in this case $p = 2$. The output rotational speed n_1 of the electric motor is therefore equal to:

$$n_1 = \frac{60\,f}{p} = 30f \;\; [rpm] \tag{6.1}$$

At this point the main problem is that the electric motor, in order to avoid losses by working in optimal conditions, needs higher rotational speeds than a few tens of rpm which would cause, even if the prototype is tested at low speeds, several vibrations in the system. It is therefore necessary to use a speed reducer from position between the output of the electric motor and the shaft connected to the wheel, in this way substantial rotational speeds for the engine will be less dangerous for the stability and safety of the prototype. A speed reducer present in the Laboratory with a reduction ratio $\tau = \frac{n_1}{n_2} = 2.89$ was used and the rotation speed of the wheel is calculated in according to (6.2) where f is the user input parameter for the frequency in the AC-drive. In figure 6.4 a scheme of the connection between the electric motor and the gearbox is showed and in figure 6.5 a picture of the final prototype is presented.

$$n_2 = \frac{30f}{\tau} = 10.38f \;\; [rpm] \tag{6.2}$$

In figure 6.6 an overview with different input frequencies is presented, where v_2 is the tangential speed of the wheel (the effective speed of the EV) and is calculated as in equation (6.3), r is the radius of the wheel, ω_1 and ω_2 are respectively the output angular speed of the motor and the output angular speed of the gearbox

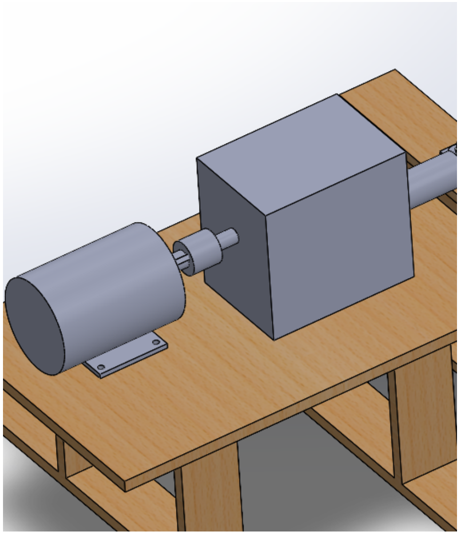

Figure 6.4: Motor-reducer connection

Figure 6.5: Final inWIPT prototype

(the same of the wheel). In figure 6.7 is presented a graph where the input/output parameters of the system are showed: the linear speed of the wheel is characterized as function of the frequency of the AC-driver.

$$v_2 = 3.6\, r\, n_2 \;\; [km/h] \tag{6.3}$$

6.2.2 Wire support

In order to make the prototype more manageable, making any changes in the shortest possible time, it was important to redesign the support for the wires that make up the coils on the outer surface of the wheel. The initial support, visible in figure 6.3, was made of wood with holes through for the wire so in case of breakage, damage or any other need to disassemble the operations would be particularly slow and laborious. The purpose is to create through Solidworks a new type of support to be printed by 3D printer in order to facilitate the assembly and disassembly of wires. The wheel has a length of 25 cm so the idea is to put a couple of supports at the two side of it.

The first two printed versions were made starting from nominal size of the wire that has a diameter of 3.5 mm and modifying them by try and error procedure. In particular, the goal is to create a hole with a not closed section to insert the wire into it with a simple pressure of the finger. Some attempts of holes are shown in

f [Hz]	n1 [rpm]	ω1 [rad/s]	n2 [rpm]	w2 [rad/s]	v2 [km/h]
2	60	6,3	20,8	2,2	2,0
4	120	12,6	41,5	4,3	3,9
6	180	18,8	62,3	6,5	5,9
8	240	25,1	83,0	8,7	7,8
10	300	31,4	103,8	10,9	9,8
12	360	37,7	124,6	13,0	11,7
14	420	44,0	145,3	15,2	13,7
16	480	50,3	166,1	17,4	15,7
18	540	56,5	186,9	19,6	17,6
22	660	69,1	228,4	23,9	21,5
26	780	81,7	269,9	28,3	25,4
30	900	94,2	311,4	32,6	29,4
34	1020	106,8	352,9	37,0	33,3
38	1140	119,4	394,5	41,3	37,2
42	1260	131,9	436,0	45,7	41,1
46	1380	144,5	477,5	50,0	45,0
50	1500	157,1	519,0	54,4	48,9

Figure 6.6: Output speed with different input f

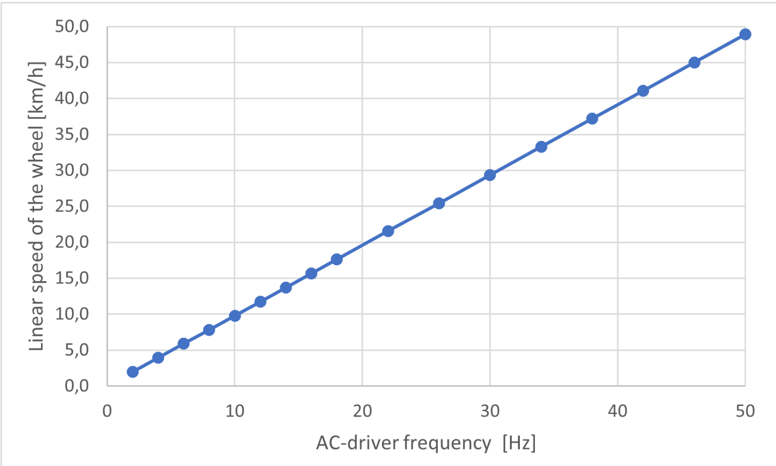

Figure 6.7: Linear speed of the wheel as function of f

the figure 6.8. The final version of the support is showed in figure 6.9. It has a base surface of 15x120 mm and an height of 5 mm. The hole shape is totally custom for the wire and the rule of the vertical hole is to fix the support to the wheel.

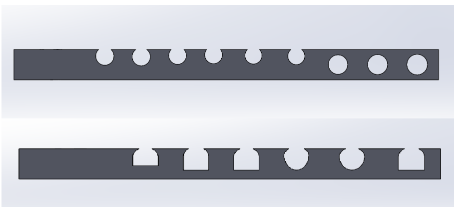

Figure 6.8: Attempts of different hole shape

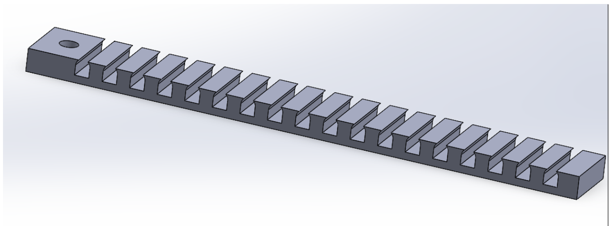

Figure 6.9: Final version

Chapter 7

CONCLUSIONS AND FUTURE WORK

7.1 Conclusions

From the results of chapter 5 it is evident that to have a good transfer of energy in a IPT system one of the most crucial parameters is the air-gap. It is important to have an AG as close as possible to the nominal one, with an AG double of the nominal one the value of mutual inductance and coupling factor decrease also of 70%. The area below the graphs decreases considerably with the variation of the AG, this means that much less energy is transferred. Therefore it is important to consider a solution that guarantees constant air-gap with vehicles of different heights both in static and dynamic situations. For the static it is easier, since the EV is parked, solve this problem putting the primary pad on a mobile platform that is able to move, also in an autonomous way using some proximity sensors, above and below in order to have the same AG with every kind of EV. The mobile platform could also be placed on the EV, moving so the secondary pad. It would make the vehicle more expensive so it is easier to place it on few charging station that on many EVs but this solution works very well in dynamic situation, where the vehicle spends a few fractions of a second on a pad and then move on to the next. Another solution, to avoid a mechanical system like that described, is to use a control technique in the power converter to compensate the misalignment.

For the distance between primary pads it is important to make assessments at the time of road design so as to avoid that the mutual inductance and coupling factor go to zero in the middle between two pads. Here the focus is only on this aspect since the variation of PD does not affect in significant way the energy transferred since the area below the graph changes very little.

Similar conclusions are possible also for taking into account the effect of changing the lateral misalignment: there is a critical misalignment to avoid because the coupling factor is equal to zero. For the rest is a more or less linear behavior so, in order to have a good energy transfer, is important to stay as close as possible to the central point. This is helped by the Electronic Stability Control (ESP) system able to avoid the skidding, or sensors capable of following a line: they could arrange, independently, the trajectory of the vehicle in order to always have the optimal lateral position.

7.2 Future work

The best way to mitigate the problem of air-gap in a EV charged with IPT is to have an In-wheel system but the technology is still very young. One of the future works could be improve this charging system, working in particular on the distribution of the coils on the surface.

An important improvement should be done on the inWIPT prototype where in the current configuration is not able to simulate the motion of pure rolling between the wheel and the ground in fact not translation is present, but just a rotational one. It is very important to obtain reliable results in case of dynamic analysis of the inWIPT system.

To continue this work some of these suggestions can be taken:

- Evaluate the impact of electromagnetic radiation in dynamic IPT and study ways of minimizing it
- Repeat experiments using different operating frequency
- Repeat experiments with a real-scale prototype
- Characterization of magnetic coupler carried out in this thesis is only a part of the entire EVs wireless charging systems. Reduced order model of wireless charging systems is used to determine the power transfer efficiency. A complete circuit consisting of individual power electronic devices from the grid to the vehicle can also be studied in the future.
- Study an optimal way to simulate the pure rolling motion in the inWIPT prototype.

Appendix A

Skin effect

The skin effect happens in conductors of alternating current (AC). As AC current flows through a copper wire, the fluctuating magnetic field it creates generates conflicting eddy currents. Eddy currents occur more densely near the conductor's surface so, in according with the second Ohm law (A.1), if the cross area reduces the resistance of the conductor increases.

$$R = \frac{\rho}{A} l \tag{A.1}$$

Skin depth decreases with as frequencies are reduced, making this issue more common in high-frequency applications.By using multiple wires within one cable, however, litz wire minimizes this effect by distributing AC current throughout the entirety of the wire rather than letting it travel along the surface. Using thinner copper wires ensure that each unique strand possesses a smaller radius than the skin depth. As such, the diameter of each copper wire must be smaller, correlating directly with the height of the frequency

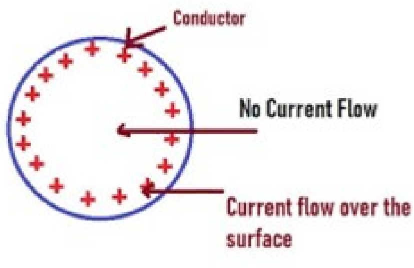

Figure A.1: Skin effect

Figure A.2: Litz wire

Appendix B

Coupling factor graphs

The graphs of the coupling factor k in the case of changing lateral displacement between primary and secondary pads are here presented. The shape is the same of mutual inductance M.

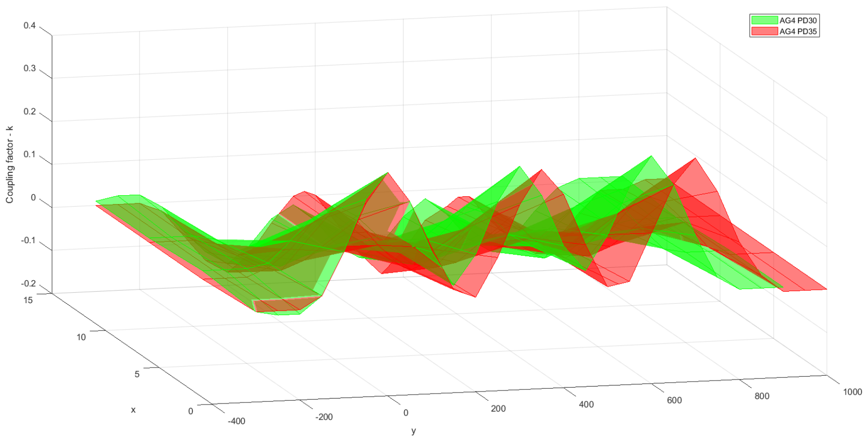

Figure B.1: k, 4 cm air gap with different primary distances

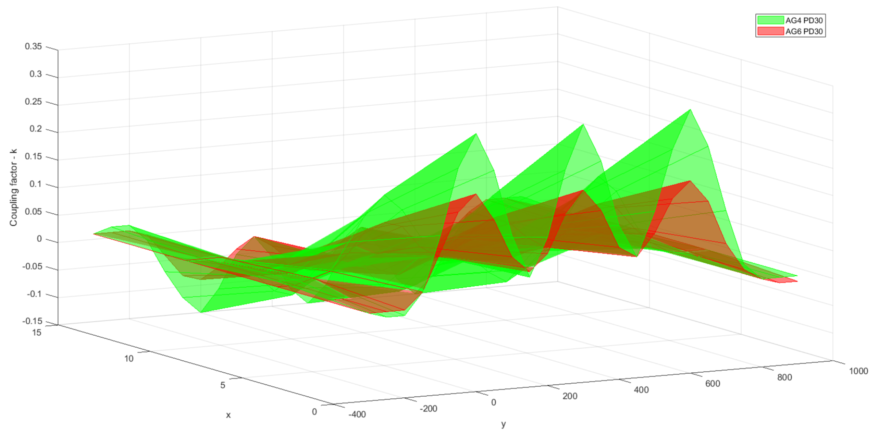

Figure B.2: k, different air-gaps with 30 cm primary distance

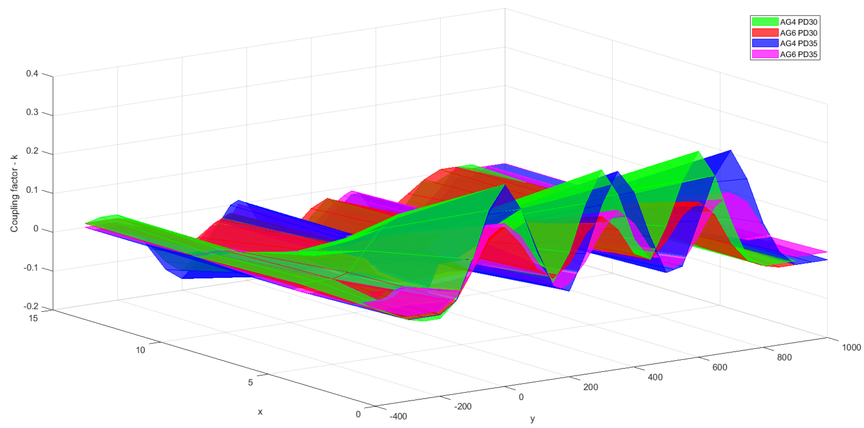

Figure B.3: k, complete graph

Bibliography

[1] Wikipedia. *History of the electric vehicle.* [Last update on July 2022]. 2022. URL: https://en.wikipedia.org/wiki/History_of_the_electric_vehicle (cit. on p. 1).

[2] Valter S. Costa, Emanuel Marques, Andre Pereira Mendes, Marina S. Perdigao, and Andre M. S. Mendes. «Magnetic Couplers for Dynamic IPT Systems». In: (2019), pp. 1–6 (cit. on pp. 1, 16, 17, 34).

[3] EconomyUp. *Mobilità elettrica 2021, raddoppiano i mezzi elettrici circolanti. Tre scenari per il futuro.* [Data from Smart Mobility Report 2021 of Osservatorio Smart Mobility (Polimi)]. October 2021. URL: https://www.economyup.it/mobilita/mobilita-elettrica-2021-raddoppiano-i-mezzi-elettrici-circolanti-tre-scenari-per-il-futuro/ (cit. on p. 3).

[4] EU. *Emissioni di CO2 delle auto: i numeri e i dati.* [Last update june 2022]. March 2019. URL: https://www.europarl.europa.eu/news/it/headlines/society/20190313STO31218/emissioni-di-co2-delle-auto-i-numeri-e-i-dati-infografica (cit. on pp. 3, 5).

[5] Wikipedia. *Auto elettrica.* [Last update on July 2022]. 2022. URL: https://it.wikipedia.org/wiki/Auto_elettrica (cit. on pp. 4, 5).

[6] EVgo. *Types of Electric Vehicles.* A brief overview of EV options. 2022. URL: https://www.evgo.com/ev-drivers/types-of-evs/#40 (cit. on p. 6).

[7] LUCIAN MIHET-POPA AGANTI MAHESH BHARATIRAJA CHOKKALINGAM. «Inductive Wireless Power Transfer Charging for Electric Vehicles–A Review». In: (2021), pp. 1–2 (cit. on pp. 7, 9, 10).

[8] Detroit Free Press MARK PHELAN. *L'auto elettrica da 1000 km con una ricarica? L'abbiamo provata.* [Adapted by Massimo Grassi]. April 2022. URL: https://it.motor1.com/reviews/580137/mercedes-eqxx-concept-prova-autonomia/ (cit. on p. 7).

[9] Carplug. *WHICH CHARGING CABLE TO CHOOSE FOR MY ELECTRIC CAR?* 2022. URL: https://www.carplug.eu/which-charging-cable-for-electric-car (cit. on p. 8).

[10] Wikipedia. *Wireless power transfer*. [Last update on August 2022]. 2022. URL: https://en.wikipedia.org/wiki/Wireless_power_transfer (cit. on pp. 9, 10, 13, 20).

[11] André Pereira Mendes. «Wireless power transfer system for continuous charging of electric vehicles». MA thesis. Universidade de Coimbra: Faculdade de ciencias e tecnologia, 2017 (cit. on p. 13).

[12] Juan Luis Villa. «Wireless Power for Electric Vehicles». PhD thesis. Torino: Politecnico di Torino (cit. on pp. 18, 19).

[13] Rakan Chabaan Aqueel Ahmad Mohammad Saad Alam. «A Comprehensive Review of Wireless Charging Technologies for Electric Vehicles». In: (2018), p. 3 (cit. on p. 19).

[14] Hemant Kumar Dashora. «Dynamic Wireless Charging of Electric Vehicle». PhD thesis. Italy: University of Padova. URL: https://www.research.unipd.it/retrieve/e14fb26f-b300-3de1-e053-1705fe0ac030/Dashora_Hemant_Kumar_thesis.pdf (cit. on p. 20).

[15] Anna De Simone. *L'Autobus elettrico che si ricarica alla fermata.* [] 2012. URL: https://www.ideegreen.it/lautobus-elettrico-che-si-ricarica-alla-fermata-13293.html (cit. on p. 21).